Longitudinal follow-up and characterization of a robust rat model for Parkinson's disease based on overexpression of alpha-synuclein with adeno-associated viral vectors.

By Van der Perren A, Toelen J, Casteels C, Macchi F, Van Rompuy AS, Sarre S, Casadei N, Nuber S, Himmelreich U, Osorio Garcia MI, Michotte Y, D'Hooge R, Bormans G, Van Laere K, Gijsbers R, Van den Haute C, Debyser Z, Baekelandt V.

Published in Neurobiol Aging. 2015 Mar;36(3):1543-58.
doi: 10.1016/j.neurobiolaging.2014.11.015.

Longitudinal follow-up and characterization of a robust rat model for Parkinson's disease based on overexpression of alpha-synuclein with adeno-associated viral vectors.

Authors:

Anke Van der Perren[1], Jaan Toelen[2], Cindy Casteels[3], Francesca Macchi[1], Anne-Sophie Van Rompuy[1], Sophie Sarre[4], Nicolas Casadei[5], Silke Nuber[5,6], Uwe Himmelreich[7], Maria Isabel Osorio Garcia[7], Yvette Michotte[4], Rudi D'Hooge[8], Guy Bormans[9], Koen Van Laere[3], Rik Gijsbers[2,10], Chris Van den Haute[1,10], Zeger Debyser[2,10], Veerle Baekelandt[1,10]

Affiliations:

[1] *KU Leuven, Laboratory for Neurobiology and Gene Therapy, Department of Neurosciences, Flanders, Belgium*

[2] *KU Leuven, Molecular Virology and Gene Therapy, Department of Pharmaceutical and Pharmacological Sciences, Flanders, Belgium*

[3] *Leuven University Hospital and KU Leuven, Division of Nuclear Medicine, Belgium*

[4] *Vrije Universiteit Brussel, Department of Pharmaceutical Chemistry and Drug Analysis, Belgium*

[5] *University of Tübingen, Institute of Medical Genetics and Applied Genomics, Germany*

[6] *University of California San Diego, Department of Psychiatry, USA*

[7] *KU Leuven, Biomedical MRI Unit, Belgium*

[8] *KU Leuven, Laboratory of Biological Psychology, Department of Psychology, Tiensestraat 102, 3000, Leuven, Belgium*

[9] *KU Leuven, Laboratory for Radiopharmacy, Belgium*

[10] *KU Leuven, Leuven Viral Vector Core, Leuven, Belgium*

Correspondence:

Veerle Baekelandt, Kapucijnenvoer 33 - VCTB+5

B-3000 Leuven, Flanders, Belgium. Tel 32-16-33 21 94 - Fax +32-16-33 63 36

E-mail: Veerle.Baekelandt@med.kuleuven.be

Abstract

Testing of new therapeutic strategies for Parkinson's disease (PD) is currently hampered by the lack of relevant and reproducible animal models. Here, we developed a robust rat model for PD by injection of adeno-associated viral vectors (rAAV2/7) encoding α-synuclein into the substantia nigra, resulting in reproducible nigrostriatal pathology and behavioral deficits in a 4 weeks time period. Progressive dopaminergic dysfunction was corroborated by histopathological and biochemical analysis, motor behavior testing and *in vivo* microdialysis. L-DOPA treatment was found to reverse the behavioral phenotype. Non-invasive PET imaging and MR spectroscopy allowed longitudinal monitoring of neurodegeneration. In addition, insoluble α-synuclein aggregates were formed in this model. This α-synuclein rat model shows improved face and predictive validity, and therefore offers the possibility to reliably test novel therapeutics. Furthermore, it will be of great value for further research into the molecular pathogenesis of PD and the importance of α-synuclein aggregation in the disease process.

Introduction

Parkinson's disease (PD) is a progressive, age-related neurodegenerative movement disorder affecting about 1–2% of people above 60 years (Wirdefeldt et al., 2011). Both genetic and environmental factors are believed to play a causal role in the onset of PD, but to date, the exact etiology and underlying molecular mechanisms remain unclear. The pathophysiology of PD is characterized by the selective and progressive loss of dopaminergic neurons (DN) in the *substantia nigra pars compacta* (SNpc) resulting in a striatal depletion of dopamine (DA). The resident neurons contain α-synuclein-positive intracellular inclusions designated as Lewy bodies (LBs) and dystrophic neurites called Lewy neurites (LNs) (Forno, 1996). α-Synuclein, a protein of 140 amino acids localized in nerve terminals, is the major protein present in fibrillar form in LBs and LNs in sporadic and inherited PD (Spillantini et al., 1997). Moreover, genetic aberrations in the *SNCA* gene encoding human α-synuclein, such as point mutations (A53T, A30P, E46K), duplications and triplications, are the cause of autosomal dominant forms of PD (Polymeropoulos et al., 1997, Kruger et al., 1998, Singleton et al., 2003, Chartier-Harlin et al., 2004, Ibanez et al., 2004, Zarranz et al., 2004). Very recently, two new mutations in human α-synuclein (G51D and H50Q) have been linked to PD (Appel-Cresswell et al., 2013, Kiely et al., 2013, Lesage et al., 2013). The physiological function of α-synuclein and the mechanisms leading to aggregation and selective degeneration of nigral neurons are still not well understood.

To study the pathophysiology of PD and to develop novel therapeutic strategies, there is an urgent need for animal models that more closely resemble the neuropathology, physiology and motor symptoms of human PD, and therefore might have a higher predictive value to translate new therapies from animal models to patients. Glial cell line-derived neurotrophic factor (GDNF) for example, is neuroprotective in the commonly used neurotoxin models of PD, but was shown to lack neuroprotective efficacy in viral vector-mediated α-synuclein

models (Lo Bianco et al., 2004, Decressac et al., 2011); this might explain the poor outcome so far in clinical trials with GDNF in PD patients (Marks et al., 2010). Moreover, new therapeutic avenues targeting α-synuclein aggregation and/or neurotoxicity require robust α-synuclein-based animal models. Overexpression of both wild type (WT) and several clinical mutants of human α-synuclein in transgenic mice has been shown to induce pathological accumulation of α-synuclein and neuronal dysfunction (Masliah et al., 2000, Kahle et al., 2001, Fleming et al., 2005, Freichel et al., 2007, Chesselet et al., 2011). However, until now transgenic α-synuclein mouse models failed to display clear age-dependent dopaminergic cell loss and associated behavioral deficits (reviewed by Magen and Chesselet (Magen et al., 2010)).

This hurdle was overcome by direct targeting of the *substantia nigra* (SN) with viral vectors overexpressing α-synuclein. Both lentiviral (LV) and recombinant adeno-associated viral (rAAV) vectors encoding human α-synuclein have been explored for this purpose (reviewed in (Löw, 2012, Van der Perren et al., 2014)), but rAAV vectors are particularly attractive to target the SN due to their high transduction efficiency and tropism for dopaminergic neurons (Taymans et al., 2007, Van der Perren et al., 2011). Several rAAV serotypes (rAAV2/2, 2/5, 2/6 and 1/2) have been applied to overexpress α-synuclein in the rat, mouse and primate brain (Kirik et al., 2002, Klein et al., 2002, Yamada et al., 2004, Eslamboli et al., 2007, St Martin et al., 2007, Gorbatyuk et al., 2008, Azeredo da Silveira et al., 2009, Koprich et al., 2011). These models exhibit different key features of the human disease such as nigral dopaminergic cell loss, α-synucleinopathy in surviving neurons and dopamine-related motor deficits. However, the observed nigral cell loss as well as the time course described has been quite variable. Due to this variation, the lack of overt behavioral impairments is a shortcoming of most current rAAV-based α-synuclein models (reviewed in (Ulusoy et al., 2010, Löw, 2012, Van der Perren et al., 2014)).

In this study, we aimed to establish a viral vector-based rat model for PD with robust and reproducible nigrostriatal pathology that allowed detection of behavioral deficits in a relatively short time period. Therefore, we stereotactically injected rAAV2/7 encoding the human A53T α-synuclein mutant in the SN of adult rats. Progressive dopaminergic dysfunction and α-synuclein aggregation were assessed by histopathological and biochemical analysis, non-invasive PET imaging, MR spectroscopy, microdialysis and motor behavior.

Materials and methods

Recombinant AAV production and purification

Vector production and purification was performed as previously described (Van der Perren et al., 2011). The plasmids include the constructs for the AAV7 serotype, the AAV transfer plasmid encoding the human A53T mutant or WT α-synuclein or the eGFP transgene under the control of the ubiquitous CMVie enhanced synapsin1 promoter and the pAdvDeltaF6 adenoviral helper plasmid. Real-time PCR analysis was used for genomic copy determination.

Stereotactic injections

All animal experiments were carried out in accordance with the European Communities Council Directive of 24 November 1986 (86/609/EEC) and approved by the Bioethical Committee of the KU Leuven (Belgium). Young adult female Wistar rats (Janvier, France) weighing about 200-250 g were housed under a normal 12 h light/dark cycle with free access to pelleted food and tap water. All surgical procedures were performed using aseptic techniques and ketamine (60 mg/kg ip., Ketalar®, Pfizer, Belgium) and medetomidine (0.4 mg/kg, Dormitor®, Pfizer) anaesthesia. Following anaesthesia the rodents were placed in a stereotactic head frame (Stoelting, IL, USA). Injections were performed with a 30-gauge needle and a 10-µl Hamilton syringe. All animals were injected with 3 µl A53T α-synuclein rAAV2/7 (low: 3.0E+10 GC/ml, standard: 3.0E+11 GC/ml or high: 1.0E+12 GC/ml vector dose). Stereotactic coordinates used for the SN were anteroposterior (AP) -5.3, lateral (LAT) -2.0, dorsoventral (DV) -7.2, calculated from the dura using bregma as reference. The injection rate was 0.25µl/min, the needle was left in place for an additional 5 min before being retracted. Control animals were injected with eGFP rAAV2/7 (standard: 3.0E+11 GC/ml vector dose) or 6-OHDA (Sigma; calculated as free base, 25µg dissolved in 3 µl of 0.05%

ascorbate saline) into the SN using the same coordinates. The 6-OHDA solution was kept on ice, used fresh, and protected from light to minimize oxidation.

Histology

Rats were sacrificed with an overdose of sodium pentobarbital (60 mg/kg, i.p., Nembutal®, Ceva Santé, Belgium) followed by intracardial perfusion with 4% paraformaldehyde in PBS. After postfixation overnight, 50 µm thick coronal brain sections were made with a vibrating microtome (HM 650V, Microm, Germany). IHC was performed on free-floating sections using an antibody against α-synuclein (rabbit polyclonal 1:5000, Chemicon 5038). This antibody can detect both human and rat α-synuclein, but endogenous levels of rat α-synuclein were below detection limits within nigral cell somata, owing to its predominant localization at synaptic membranes. We also used antibodies against TH (rabbit polyclonal 1:1000, Chemicon 152) and VMAT (rabbit polyclonal 1:1000, Abcam 81855). Sections were pretreated with 3% hydrogen peroxide for 10 min and incubated overnight with primary antibody in 10% normal goat or swine serum (DakoCytomation, Belgium). As secondary antibody we used biotinylated anti-rabbit IgG (1:600 (α-synuclein), 1:300 (other antibodies) DakoCytomation), followed by incubation with streptavidin–horseradish peroxidase complex (1:1000, DakoCytomation). α-synuclein and VMAT2 immunoreactivity were visualized using 3,3-diaminobenzidine (0.4 mg/ml, Sigma-Aldrich) and TH immunoreactivity was visualized using Vector SG (SK-4700, Vector Laboraties, CA) as a chromogen.

For fluorescent double staining, sections were rinsed three times in PBS and then incubated overnight in PBS-0.1% triton X-100, 10% goat serum, and the following antibodies: rabbit anti-α-synuclein (1:1000, Chemicon 5038) and mouse anti-TH (1:1000, Calbiochem 6D7), or mouse anti P-S129 α-synuclein (1:1000, Elan Pharmaceuticals) and rabbit anti-TH (1:1000, Chemicon 152), or rabbit anti-NeuN (1:1000, Millipore ABN78) and chicken anti TH

(1:1000, Aves TH1205), or mouse anti- α-synuclein (1:100, Invitrogen LB309) and rabbit anti-Ubiquitin (1:1000, Dako 20458). After three rinses in PBS-0.1% triton X-100 the sections were incubated in the dark for 1 h in fluorochrome-conjugated secondary antibodies: goat anti-rabbit Alexa 488 (1:500, Molecular Probes™, Invitrogen, Belgium) and goat anti-mouse Alexa 633 (1:500, Molecular Probes™, Invitrogen). After being rinsed in PBS and mounted, the sections were coverslipped with mowiol. Fluorescent double staining were visualized by confocal microscopy with an LSM 510 unit (Zeiss, Belgium).

Stereological quantification

The number of TH-positive cells and α-synuclein positive cells in the SN was determined by stereological measurements using the Optical fractionator method in a computerized system as described before (Baekelandt et al., 2002) (StereoInvestigator; MicroBright-Field, Magdeburg, Germany). Every fifth section throughout the entire SN was analyzed, with a total of seven sections for each animal. The coefficients of error, calculated according to the procedure of Schmitz and Hof as estimates of precision (Schmitz et al., 2005) varied between 0.05 and 0.10. The volume of α-synuclein expression in the brain and the SN was determined by the Cavalieri method. Every fifth section covering the entire extent of the SN, with a total of seven sections for each animal, was included in the counting procedure. The coefficients of error varied between 0.05 and 0.14. We quantified both the injected and non-injected SN (internal control), no cell loss was observed in the non-injected side. All the analyses were performed by an investigator blind to different groups.

Behavioral testing

Cylinder test

The cylinder test was used to quantify forelimb use. Contacts made by each forepaw with the wall of 20-cm-wide clear glass cylinder were scored from the videotapes by an observer blinded to the animal's identity. A total of 20 contacts were recorded for each animal. The number of impaired forelimb contacts was expressed as a percentage of total forelimb contacts. Non-lesioned control rats should score around 50% in this test. To study the response to dopaminergic treatment, rats were injected intraperitoneally with L-DOPA (Roche, Prolopa 125, 6 mg/kg) 45 minutes prior to the cylinder test. All the analyses were performed by an investigator blind to different groups.

Skilled paw reaching test

Forepaw reaching and grasping was assessed using the skilled paw reaching test. Briefly, a double staircase (accessible with the left and right forepaw) consisting of seven graded stages of reaching difficulty was baited with four sugar pellets per step (28 on each side). The rats were deprived of food (12 gram per rat per day) to about 90% of their initial body weight. In the first 4 days the rats were familiarized with the test and the sucrose pellets were available for 15 minutes. In the test session the animals were placed inside the box and had only 5 minutes to reach, retrieve and eat the sucrose pellets. This was repeated 3 times. After each test session the numbers of remaining pellets on each stair were counted. This test was performed 6 weeks after injection.

Open field

The open field test was used to assess locomotor behavior. After putting the rat in the dark for 30 minutes, the animal was placed in the center of the square and was allowed to explore the area for 10 minutes, following 1 minute of adaptation. Using tracking software (Ethovision Noldus) the total distance traveled was recorded. This test was performed 4 days, 15 days and 28 days after injection.

Rotarod

The motor performance was assessed using rotarod equipment. First the animals were trained prior to injection in order to reach stable performance. The training consisted of 4 trials of 6 minutes with at least 5 minutes of rest between the trials with an initial speed of 12 rpm, after 3 minutes the rotational speed of the test was increased to 18 rpm. After this initial training, the rats were subjected to the test and the latency to fall was recorded. This test was performed 4 days, 15 days and 28 days after rAAV2/7 α-synuclein injection. Since no differences were detected between the two groups, the rats were subjected 6 weeks after injection to a rotarod reaching a higher speed (Rotarod Advanced TSE systems). The rats were placed on a rod with an increasing speed of 4 rpm to 40 rpm over a 100 sec period.

Small animal PET Imaging

Dopamine transporter imaging was done using the radioligand [^{18}F]-FECT [(2'-[^{18}F] fluoroethyl (1R-2-exo-3-exe)-8-methyl-3-(4-chlorophenyl)-8-azabicyclo[3.2.1]-octane-2-carboxylate] (Wilson et al., 1996, Prasad et al.). The synthesis of [^{18}F]-FECT radiotracer was performed according to the procedure by Wilson *et al*. but using 2-^{18}F-fluoroethyltrifluoromethanesulfonate instead of 2-^{18}F-fluoroethylbromide (Wilson et al., 1996).

Small-animal PET imaging was performed using an LSO detector-based FOCUS 220 tomograph (Siemens/Concorde Microsystems, Knoxville, TN), which has a transaxial resolution of 1.35 mm full-width at half-maximum. Data were acquired in list mode in a 128x128x95 matrix with a pixel width of 0.475 mm and a slice thickness of 0.796 mm. Prior to small-animal PET imaging, rats were anesthetized using ketamine (60 mg/kg ip., Ketalar®, Pfizer, Belgium) and medetomidine (0.4 mg/kg, Dormitor®, Pfizer) anaesthesia. Tail veins were catheterized for infusion of [^{18}F]-FECT: 26.5 ± 3.7 MBq (specific activity range: 53 – 760 GBq/µmol; injection volume 500µl). [^{18}F]-FECT measurements were obtained during 40

min, starting 3 h post injection, as previously described (Casteels et al., 2006). Sinograms were reconstructed using filtered backprojection (FBP). No corrections were made for attenuation and scatter.

Parametric DAT binding potential (BP) images were constructed by reference to the cerebellum: (average tissue/ average cerebellum activity concentration)-1. For each subject, these parametric BP images were spatially normalized to a stereotactic space based upon the rat brain Paxinos atlas (Paxinos and Watson, 1998), and subsequently analyzed using a predefined volume-of-interest (VOI) approach (Casteels et al., 2006). For DAT impairment, the affected-to-non-affected side BP ratio was obtained.

Magnetic resonance imaging

For *in vivo* MRI experiments, anaesthesia was induced in an induction chamber with 3-4% isoflurane in 100% oxygen and maintained in the MRI scanner at 1-2% in 100% oxygen. Respiration and body temperature were monitored throughout the measurements and maintained at 37°C and 60-80 min^{-1}, respectively. MR images were acquired using a 9.4 T Biospec small animal MRI scanner (Bruker Biospin, Ettlingen, Germany) with a horizontal bore of 11.7 cm and equipped with actively shielded gradients (600 mT m^{-1}). A 7.2 cm linearly polarized resonator for transmission and an actively-decoupled, circular polarized rat head surface coil for receiving (both Bruker Biospin) were used. After acquisition of 2D multi-slice localizer images, 2D multi-slice-multi-echo experiments were acquired for the calculation of T_2 maps to assess edema or lesion formation (acquisition parameters: TR=4,000ms, 10 TE increments of 10 ms, 8 dummy scans, 256^2 matrix, 3.5 x 3.5 cm field-of-view, 0.5 mm slice thickness, 20 continuous slices with interlaced acquisition). High resolution 3D T_2*-weighted MR images (FLASH, TR=100 ms, TE=12 ms, flip angle 30°, 4.0 x 2.6 x 1.3 cm field-of-view, 100 μm isotropic resolution, flip angle 20°), resulting in an

isotropic resolution of 100 μm were acquired. Images were processed using Paravision 5 (Bruker Biospin).

Magnetic resonance spectroscopy

Single voxel 1H MR spectroscopy was performed as previously described (Osorio-Garcia et al., 2011, Osorio-Garcia et al., 2011). In brief, the PRESS pulse sequence with implemented pre-delay outer volume suppression as well as the water suppression method VAPOR were used. MRS parameters were: TR = 2s, TE = 20ms, SW = 4 KHz and 256 averages. Volumes of interest (voxel) were 2 × 2 × 1.5 mm^3 and placed around the SN. Spectra were corrected for B0 instability due to eddy currents as well as B0 drift using the Bruker built-in routines. Shimming was performed using FASTMAP for initial shimming and subsequent manual shimming on the selected volume performed, which resulted in a final water line width of < 25 Hz.

MR spectra were processed according to (Osorio-Garcia et al., 2011, Osorio-Garcia et al., 2011) using the jMRUI software. This included filtering out the residual water located, phase correction and baseline correction. Signal quantification was performed using AQSES by fitting a linear combination of metabolite profiles to the experimental data and the modeling of the baseline using splines (Poullet et al., 2007). The basis set of metabolites included alanine, aspartate, creatine, γ-aminoburytic acid, glucose, glutamine, glutamate, glycerolphosphorylcholine, glutathione, lactate, myo-inositol, *N*-acetyl aspartate, phosphorylcholine, phosphocreatine, phosphoryl ethanolamine and taurine. The unsuppressed water signal was acquired with identical parameters except for the acquisition of only one average, a higher receiver gain and TR=10s. The unsuppressed water was used as an internal standard for the quantification of metabolites.

Microdialysis

Microdialysis experiments were performed on rats 4, 15 and 28 days following intranigral injection of A53T α-synuclein rAAV2/7. The rats were anaesthetized with a mixture of ketamine: diazepam (50 mg/kg: 5 mg/kg i.p.) and placed in a stereotaxic frame. The skull was exposed and a burr hole was drilled to implant a guide cannula (MAB 2/6/9.14.IC, Microbiotech/se AB, Stockholm, Sweden) positioned 3 mm above the right dorsal STR according to the atlas of Paxinos and Watson (1986) (coordinates relative to bregma: L: −2.4, A: +1.2 and V: +2.8). The animals received ketoprofen (4 mg/kg i.p.; Ketofen®) as analgesic. After surgery, a probe (MAB 6.14.3, Microbiotech/se AB) with a membrane length of 3 mm and a molecular weight cut off value of 15 kDa was introduced via the cannula. The probe was perfused with modified Ringer's solution containing 147 mM NaCl, 4 mM KCl and 1.1 mM $CaCl_2$ at a constant flow-rate of 2 µl/ min using a microdialysis pump (CMA 100; CMA Microdialysis, Stockholm, Sweden). Animals were allowed to recover from surgery overnight and dialysate collection was started the next day.

Samples were collected every 20 min. Before any pharmacological manipulation was performed, four dialysate samples were collected. The mean of these neurotransmitter dialysate concentrations was taken as basal value at time zero. For i.p. injection, 2.73 mg *d*-amphetamine sulfate to obtain 2 mg *d*-amphetamine was dissolved in 1 ml saline and 1 ml/kg was administered immediately after the baseline samples had been obtained (time 20 min). At time point 200 min, when baseline levels were reached, TTX (1 µM) dissolved in Ringer's solution was administered locally by perfusion through the microdialysis probe for another 4 collections (1hour and 20 min) in order to determine the exocytotic nature of the DA release in these animals (Sarre et al., 2004).

Determination of dialysate DA levels was performed by microbore liquid chromatography (LC) as described previously (Sarre et al., 2004). In summary, the assay of DA was based on ion-pair reversed-phase (C8) LC, coupled to amperometric detection (Decade, Antec, Leiden,

The Netherlands). The mobile phase consisted of 28 ml acetonitrile and 200 ml of the following buffer: 0.1 M sodium acetate trihydrate, 20 mM citric acid monohydrate, 2 mM decane sulfonic acid and 0.5 mM sodium EDTA adjusted to pH 5.5. The oxidation potential was set at + 450 mV. The limit of detection (LOD) of the assay was 0.04 nM. To establish the extent of DA depletion in STR, the method described by Izurieta-Sanchez *et al*. (Izurieta-Sanchez et al., 1998) was used. Tissue DA content was expressed as micrograms of DA per g wet weight (WW) of tissue. The limit of detection of the LC system corresponds to a residual tissue DA content of less than 0.05 ng per g wet weight.

Western Blotting

Soluble and insoluble protein extraction:

Native nigral tissues were homogenized in Tris-buffered saline and proteins sequentially extracted, slightly modified as previously published (Tofaris et al., 2006) . Briefly, tissues were homogenized at full speed for 30 sec (VWR, ULTRA-TURRAX, T 10 basic) in 10 volumes of TBS+ (50 mM Tris-HCl, pH 7.4, 175 mM NaCl; 5 mM EDTA, protease inhibitor cocktails (Roche Complete)) and incubated for at least 1 hour on ice. Samples were spun for 30 min at 120.000 g and the resulting supernatants represented the TBS soluble fraction. The pellet was subsequently extracted in TBS+ containing 1% of Triton X-100, TBS+ containing 1 M sucrose, and RIPA buffer (TBS+, 1% NP-40, and 0.5% sodium deoxycholate, 0.1% SDS), each extraction step was followed by centrifugation for 20 min at 120.000 g. The detergent-insoluble pellet was finally solubilized in 2M urea/ 5% SDS. Samples were supplemented with 10% glycerol and stored at −80°C. For western blot analysis, 10 µg of fractionated protein extracts were used on 8–16% gradient gel (Serva, Softgel) and blotted 2 h at 80 V at 4 °C in transfer buffer (0.2 M glycine, 25 mM Tris, 10–20% methanol) on a nitrocellulose membrane (Millipore, Protran). Immunoblots were blocked in 5% dry milk in

TBS-T buffer (10 mM Tris, pH 7.5; 0.15 M NaCl; 0.1% Tween 20) and subsequently probed with anti-rodent α-synuclein (1:1000, cell signalling 4179), anti-phosphorylated alpha-synuclein (1:1000, Epitomics, 2014-1) and anti-human anti-α-synuclein (1:10, A.G. Scientific 15G7). Anti-β-actin (1:3000, Sigma, A4700) was used as internal loading control. Bound antibodies were visualized with horseradish peroxidase-conjugated secondary antibodies and enhanced chemiluminescence (ECL or ECLplus, GE Healthcare) and exposure to hyperfilm (GE Healthcare). Image were quantified using densitometry (ImageJ; NIH, USA) following 3 independent experiments.

Cross linking:

The SN was isolated and homogenized using 200 µl Tris (10 mM), EDTA (1 mM), Sucrose (0.25 mM) buffer containing proteasome inhibitor (Roche). 50 µl of the sample was used for DMSO treatment and 50 µl for DSG treatment (Thermo Scientific, 20593). 1.02 µl DSG of 50x stock was added per 50 µl sample and incubated for 30 min at 180 rpm at 37 °C. Thereafter, 2.65 µl Tris buffer 1M was added and incubated for 15 min at 180 rpm at RT to quench the activity. Finally the sample was lysed by sonication (15 sec). Total protein concentrations were determined by BCA protein assay (Thermo Scientific) according to the manufacturer's directions. Samples were prepared for electrophoresis by dilution with the respective lysis buffer, 6x loading dye and boiled for 10 min. Samples were electrophoresed on NuPAGE 4-12% Bis-Tris gels with NuPAGE MES-SDS running buffer and the PageRuler Plus molecular weight marker. After electrophoresis, gels were blotted onto PVDF membrane (Biorad) for 1h at 50V cooled in Tris (25 mM), glycine (190 mM) and methanol (20%) transfer buffer. After transfer membranes were incubated in 0.4 % paraformaldehyde for 30 min at RT, rinsed twice with PBS and once with water and blocked in 5% nonfat milk in PBS-T for 45 min. After blocking membranes were incubated with primary antibody (rat anti-human α-SYN (15G7) 1:100 or rabbit anti- α-SYN in House 1:2000) in 5% milk in PBS-T

overnight at 4°C. Anti-α-tubulin (1:50.000, Sigma) was used as internal loading control. Bound antibodies were visualized with horseradish peroxidase-conjugated secondary antibodies and enhanced chemiluminescence (ECLplus, GE Healthcare) and developed with LAS-3000 mini (Fujifilm). Densitometry analysis was performed using LAS-3000 Fujifilm software.

Results

rAAV 2/7-mediated overexpression of A53T mutant α-synuclein induces dose-dependent nigral dopaminergic cell death.

To develop a robust rat PD model we opted for the rAAV 2/7 serotype based on our previous observations that this serotype combines high transduction efficiency with high transgene expression levels in rat dopaminergic neurons (Van der Perren et al., 2011). rAAV2/7 vectors encoding the human A53T α-synuclein mutant (standard vector dose) were stereotactically injected into the right SN of adult rats. Control animals were injected with an equal dose of an eGFP encoding rAAV2/7 vector (normalized for genome copies). Four days after injection, α-synuclein and eGFP expression was detected in the SN (Fig. 1a, c). The majority (>90%) of the DN were efficiently transduced and both transgenic proteins were localized in the cell bodies and axons (Fig. 1d, e). At 29 days post injection (p.i.) a substantial reduction in α-synuclein expression was observed in the SNpc, while it was still detectable in areas surrounding the SN and eGFP expression even increased in the SNpc in the control animals (Fig. 1b, c). Western blot analysis of nigral brain extracts demonstrated a 2.2 times higher expression level compared to endogenous α-synuclein levels at 7 days p.i., increasing to 22.2 times at 29 days p.i. (Supplemental Fig. 1). Stereological quantification of the transduced volume of the SN showing α-synuclein overexpression revealed an initial increase between 4 and 8 days from 10 x 10^8 μm^3 to 33 x 10^8 μm^3, followed by a significant decrease to 10 x 10^8 μm^3 at 29 days p.i. (Fig. 1f). In contrast the transduced volume of the SN in eGFP control animals showed an initial increase at the early time points (until 17 days) followed by a stabilization of the gene expression at 29 days. (Fig. 1f). To test the specific sensitivity of dopaminergic neurons toward α-synuclein overexpression and accumulation, we also injected the vector in the striatum (STR). Injection of the rAAV 2/7 A53T α-synuclein in the STR, resulted in an initial increase in α-synuclein expression from 50 x 10^8 μm^3 at 4 days to 129.7 x

10^8 μm^3 at 17 days and was followed by a minor non-significant decrease to 94.4 x 10^8 μm^3 at 29 days (Fig. 1g).

Next, we correlated the observed kinetics of α-synuclein expression in the SN with nigral cell loss. A rapid and progressive loss of up to 80% of TH-positive neurons was detected over 29 days in rats injected with A53T α-synuclein rAAV2/7 (Fig. 2a, e). Additional stainings for vesicular monoamine transporter 2 (VMAT2) and Nissl proved genuine dopaminergic cell death rather than down regulation of tyrosine hydroxylase (TH) expression (Supplemental Fig. 2). Of note, overexpression of wild type instead of A53T α-synuclein resulted in similar dopaminergic neurodegeneration (Supplemental Fig. 3a). The loss of the DN in the SN was paralleled by a robust decrease of TH-positive nerve terminals in the STR (Fig. 2b). To rule out specific vector batch effects, different α-synuclein vector preparations were tested in the SN with similar results. No reduction in TH staining was observed in the SN or STR of eGFP rAAV2/7 injected control animals (Fig. 2c, d, e). To further investigate the dose-dependency of the onset and extent of dopaminergic neurodegeneration, we tested a 10-fold lower vector dose (low vector dose). Injection resulted in a model with slower kinetics characterized by a progressive loss of dopaminergic neurons up to 75% at 11 months after A53T α-synuclein rAAV2/7 injection (Fig. 2f).

rAAV 2/7-mediated overexpression of A53T mutant α-synuclein induces dopamine-dependent motor deficits.

To examine if the level of dopaminergic neurodegeneration was sufficient to induce motor impairments in the rats, we subjected the rats to the cylinder test to evaluate spontaneous forelimb use. From 3 weeks after injection, a significant motor impairment was seen in rats that received a standard dose of A53T α-synuclein rAAV2/7 vector. At 4 weeks after injection a 50% decrease in spontaneous contralateral (left) forepaw use was observed, whereas the

control eGFP rAAV2/7 injected animals showed no asymmetry in forepaw use (Fig. 2g). A similar asymmetric forepaw use was observed after overexpression of wild type α-synuclein (Supplemental Fig. 3b). Rats that received a higher A53T α-synuclein rAAV2/7 vector dose (high vector dose) showed a more pronounced impairment of forepaw use (70%) at 29 days after injection (Fig. 2h). To prove that the observed motor impairment was dopamine-dependent, we administered a single dose of L-DOPA to the rats injected with a high vector dose. When we repeated the cylinder test 45 minutes after L-DOPA treatment, a full recovery of the forepaw use in the A53T α-synuclein rAAV2/7 injected animals was observed (Fig. 2h). To investigate the α-synuclein induced motor deficits in more detail, a second group of animals (standard vector dose) was analysed using three extra behavioural tests at different time points after injection. First, the open-field test was applied to assess general locomotor behavior. The distance traveled in an open arena was recorded during 10 minutes. For all time points no significant difference in total distance travelled was observed between the rAAV2/7 A53T α-synuclein and rAAV2/7 eGFP vector injected animals (Fig. 3a). Second, we subjected the animals to the rotarod test to assess motor coordination and balance. The latency to fall was recorded during three test sessions with an increasing speed from 12 to 18 rpm. Since no significant differences were observed between the rAAV2/7 A53T α- synuclein and the rAAV2/7 eGPP injected animals at all time points analyzed (Fig. 3b), we switched to a more sensitive rotarod set-up (increasing speed from 4 rpm up to 40 rpm) and analyzed the rats at a later time point (6 weeks). In this case, the latency to fall was significantly lower in the rAAV2/7 A53T α-synuclein vector injected animals compared to rAAV2/7 eGFP control animals indicating impaired coordination and balance (Fig. 3c). Third, forepaw reaching and grasping was assessed using the skilled paw reaching test. Despite of a small decrease, there was no significant difference in the number of pellets successfully taken from the stairs between the rAAV2/7 A53T α- synuclein and rAAV2/7 eGFP control animals (Fig. 3d). Last,

we also subjected the animals of this second group to the cylinder test at 6 weeks p.i. Here again, a significant decrease in use of the contralateral (left) forepaw in the rAAV2/7 A53T α-synuclein injected animals was observed, confirming previous results (Fig. 3e).

PET imaging and MR spectroscopy allow non-invasive imaging of A53T α-synuclein induced progressive neurodegeneration.

To follow up the kinetics of nigrostriatal dopaminergic neurodegeneration non-invasively over time in individual animals, we quantified dopamine transporter (DAT) binding using small-animal positron emission tomography (PET) and [^{18}F]-FECT as radioligand. DAT binding significantly decreased in the ipsilateral *caudate-putamen* of A53T α-synuclein rAAV2/7 injected rats (standard vector dose) over time but remained stable in the eGFP control animal (Fig. 4a-b). Quantification of DAT binding of A53T α-synuclein rAAV2/7 injected animals showed a maximal rate of nigrostriatal dopaminergic degeneration between day 7 and 21 after injection. After 32 days, a decrease in DAT binding of up to 85% was observed (Fig. 4c). As a positive control, injection of the neurotoxin 6-OHDA in the SN induced 90% loss of DAT binding within 7 days (Fig. 4b-c).

In addition, metabolic changes were monitored as an indirect measurement of cell viability over time, using localized single voxel ^{1}H MR spectroscopy (MRS). First, magnetic resonance imaging (MRI) was used to confirm the anatomical site of injection and to exclude hemorrhages or edema formation due to the surgical procedure. Three-dimensional, high-resolution T2*-weighted MRI corroborated correct injection in the SN. At an early time point (2 days), 3 animals showed minor hemorrhages and edema near the skull, which disappeared within one or two weeks after injection and no difference was detected between the A53T α-synuclein rAAV2/7 and the eGFP rAAV2/7 injected animals (Supplemental Fig. 4a, b).

Second, metabolic changes were monitored in rAAV2/7 A53T α-synuclein and eGFP control animals over time using MRS. Voxels were centered at the SN but also included some surrounding brain tissue due to the relatively large voxel size (6 mm^3, Fig. 5a). N-acetyl aspartate (NAA) concentrations, a metabolite found in neurons, significantly decreased over time from 14 days p.i. in animals injected with A53T α-synuclein rAAV2/7 while NAA levels remained constant in eGFP control animals (Fig. 5b). A non-significant trend of decreasing glutamate and GABA concentrations was found in the A53T α-synuclein rAAV2/7 injected animals over time (Supplemental Fig. 4c, d). No changes were observed in the metabolite profiles in the contralateral hemisphere. These results demonstrate that PET imaging and MR spectroscopy can closely monitor the onset and the progression of dopaminergic neurodegeneration in individual rAAV2/7 A53T α-synuclein animals even before behavioral changes become apparent.

Nigral overexpression of A53T α-synuclein causes impaired striatal DA release.

To study the impact of α-synuclein overexpression on the function of the nigro-striatal dopaminergic pathway, we assessed changes in striatal DA content in tissue homogenates and in DA release by *in vivo* microdialysis. First, we measured the mean striatal DA content in A53T α-synuclein rAAV2/7 injected rats at 4, 15 and 28 days p.i. (standard vector dose) (Fig. 6a). Four days after injection, there was no significant difference in striatal DA content between the injected and the non-injected hemisphere. At later time points, the DA content in the affected STR time-dependently decreased to 40% and 8% of the content in the contralateral hemisphere at 15 and 28 days respectively (Fig. 6a). Striatal DA content in the contralateral hemisphere of the α-synuclein rats (intact STR) remained stable at all time points studied.

In a next step, we used microdialysis to quantify *in vivo* striatal DA release in our model. Baseline DA release, based on extracellular DA concentrations, significantly decreased over time following A53T α-synuclein rAAV2/7 injection. At 4 days, DA concentrations in the dialysates were comparable to those of intact animals, in line with earlier reports (Sarre et al., 2008). DA concentrations after nigral A53T α-synuclein rAAV2/7 injection decreased from 2.4 ± 0.89 nM at 4 days to 0.81± 0.13 nM and to 0.62 ± 0.11 nM at 15 days and 28 days p.i. respectively (Fig. 6b). These data suggest that TH-positive cell loss is preceded by a loss of striatal DA release, mimicking changes in human disease (Cheng et al., 2010).

After measuring basal DA concentrations for 20 minutes, we investigated the functionality of the remaining cells by a challenge with *d*-amphetamine (AMPH) and by local perfusion with fast sodium channel blocker tetrodotoxin (TTX). The DA levels in the striatal dialysate significantly increased up to 80 min after AMPH administration, but the peak values diminished from 42.7 ± 4.88 nM at 4 days to 15.5 ± 3.78 nM at 15 days and to 5.29 ± 1.74 nM at 28 days (Fig. 6c). After 200 min, when DA release had returned to baseline levels, TTX was administered to determine the exocytotic nature of the DA release in the rats (Sarre et al., 2004). Infusion of TTX into the SN has been shown to decrease dialysate DA to undetectable levels, suggesting that under normal conditions somatodendritic DA is released via the mechanism of exocytosis (Sarre et al., 1998). A significant decrease in dialysate levels to 25% of the baseline value was observed in all three groups 20 minutes after TTX administration (Fig. 6d). These data indicate that the striatal DA release in the A53T α-synuclein rAAV 2/7 injected rats remained TTX-dependent and imply that the measured DA levels originate from functional cells via exocytosis.

Overexpression of A53T α-synuclein induces dose- and time-dependent formation of insoluble α-synuclein positive aggregates.

Next to dopaminergic neurodegeneration, the presence of α-synucleinopathy is an important hallmark of PD. Examination of cellular morphology over time showed extensive pathology at 17 days in the A53T α-synuclein rAAV2/7 injected animals with the presence of nigral α-synuclein immunopositive cytoplasmic inclusions in the SN and bulging neurites in the STR (Fig. 7a-b). Ubiquitin immunoreactivity is a distinct feature of Lewy body pathology in the human brain (Dale et al., 1992, Dawson, 2000, Dawson et al., 2002). We observed co-localization of α-synuclein and ubiquitin at 29 days p.i. in a fraction (± 20%) of the α-synuclein expressing nigral neurons (Fig. 7c). The fibrillar nature of the α-synuclein aggregates was evaluated by Thioflavin S (Thio S) staining (LeVine, 1999). Thio S positive cells were detected in the SN from 17 days onwards (Fig. 7d). In order to further characterize the neuropathology we performed IHC staining for the phosphorylated form of α-synuclein at serine 129 (P-S129). Previous studies have shown that approximately 90% of α-synuclein in LB is phosphorylated at Serine 129, highlighting a potentially important role of this posttranslational modification in LB formation and DA cell death. We observed a significant increase in the number of P-S129 α-synuclein positive cells from 3722 ± 390 at 4 days p.i to 6207 ± 1315 at 17 days and to 7192 ± 1131 at 29 days p.i. (Fig. 7e, f, g).

Next, to examine the relation between α-synuclein aggregation and nigral neurodegeneration, we compared the number of α-synuclein positive cells in the SN with and without aggregates over time. The total number of α-synuclein positive cells in the SN increased between 4 and 8 days after injection, but decreased by 65% at 29 days (Fig. 7h). Double staining for TH and the pan-neuronal marker NeuN revealed that numerous non-dopaminergic neurons survived within the injected area, indicating that the local overexpression of α-synuclein preferentially killed dopaminergic neurons (Supplemental Fig. 5). We subsequently quantified α-synuclein

positive cells with and without aggregates. The total number of α-synuclein positive cells with aggregates initially increased over time until 17 days, before a decrease was observed. The number of α-synuclein positive cells without aggregates increased until 8 days, but decreased at 17 and 29 days (Fig. 7j). As for the ratio of aggregate–positive to aggregate–negative cells, the percentage of aggregate-positive cells increased from 20% to 50% between 8 and 17 days after injection and then stabilized at 50% (Fig. 7i). We also analyzed α-synuclein aggregation in the slower model (low vector dose) (Fig. 7k, l, m). The percentage of aggregate-positive cells increased from 10% at 4 days to 30% at 4 months, followed by stabilization at 30% up to 11 months (Fig. 7l). The overall percentage of cells with α-synuclein aggregates in the slow kinetics model at 11 months (30%) was lower than that of the fast kinetics model at 29 days (50%).

To determine the nature and solubility of the α-synuclein molecular species, we extracted the SN region of rAAV2/7 A53T α-synuclein rats at 4, 15 or 28 days p.i. Two different protocols were applied. First, α-synuclein was sequentially extracted in a soluble and insoluble fraction. We detected an increase of phosphorylated α-synuclein, while endogenous rat α-synuclein was markedly reduced over time (Fig. 8a, b, c). The detergent-insoluble α-synuclein fraction significantly increased between 4 and 28 days after injection (Fig. 8d, e). The molecular pattern associated with these insoluble α-synuclein species was composed of a major band at 15 kDa corresponding to monomeric α-synuclein, and higher bands that most likely represent dimers and other high molecular weight (HMW) oligomers possibly shifted by posttranslational modifications (ubiquitination, O-glycosylation, phosphorylation) and the typical smear, which may consist of SDS breakdown of α-synuclein fibrils (Kahle et al., 2001, Shimura et al., 2001, Anderson et al., 2006, Masliah et al., 2011). Second, we applied a recently published protocol using DSG which allows detection of higher molecular α-synuclein species via cross linking (Dettmer et al., 2013). DSG- treated brain samples of

rAAV2/7 α-synuclein injected animals revealed significantly higher levels of α-synuclein dimers (≈ 30 kDa) and other HWM oligomers (≈ 60 and ≈ 85 kDa) at 28 days p.i. compared to 7 days p.i. (Fig. 8f). In conclusion, the increase in phosphorylated and insoluble α-synuclein species over time as well as the increased levels of HMW α-synuclein oligomers at later time points, suggest a conversion of α-synuclein over time into a toxic aggregated state in this model.

Discussion

The absence of adequate animal models for PD is often put forward as the major impediment to preclinical testing of new potential treatments. The traditional toxin-based models have proven very useful to develop symptomatic dopamine-based treatments, but their validity to test disease-modifying therapies is questionable. α-Synuclein based models were subsequently developed. Most α-synuclein transgenic mouse models display prominent α-synuclein pathology, in some cases accompanied by movement disorders, but no dopaminergic cell loss, in contrast to viral vector-based α-synuclein rodent models (Chesselet, 2008, Dawson et al., 2010) however a recently generated full-length wild type a-synuclein transgenic rat model holds more promise regarding an age-dependent dopaminergic phenotype (Nuber et al., 2013). Current viral vector-based models still have shortcomings, mainly in terms of time course, robustness of the neurodegeneration and behavioral effects. In this study, we have developed, characterized and validated a viral vector-based rat model for PD, using rAAV serotype 7. Nigral delivery of A53T α-synuclein by rAAV2/7 resulted in high α-synuclein expression and concomitant loss of the nigral neurons and projecting fibers in the STR in a time- and dose-dependent manner. Injection of a standard rAAV2/7 A53T α-synuclein vector dose resulted in 80% loss of the nigral DN at 28 days p.i and was accompanied by clear behavioral deficits. Of note, overexpression of wild type α-synuclein instead of the A53T mutant resulted in similar cell loss and motor impairment, suggesting that our model is not only relevant for familial but also for sporadic forms of PD.

Previously, both LV and rAAV vectors have been explored for purposes of disease modeling. LV vectors encoding wild type, A30P or A53T mutant α-synuclein were also capable of inducing neuronal cell loss in rats, but less pronounced and more delayed (24-35% cell loss at 5 months) (Lo Bianco et al., 2002, Lauwers et al., 2007). This can be explained by the lower titers and lower transduction efficiency for DN of LV compared to rAAV vectors (Lo Bianco

et al., 2002, Lauwers et al., 2003, Lauwers et al., 2007). A first generation of rAAV2/2 based α-synuclein models displayed progressive neurodegeneration, but the loss of the nigral TH-positive neurons (25-80%) as well as the time course described, was variable (6 weeks up to 1 year) (Kirik et al., 2002, Klein et al., 2002, Yamada et al., 2004, Maingay et al., 2006, Mochizuki et al., 2006, Chung et al., 2009). Later, other rAAV serotypes notably rAAV2/5, 2/6 and rAAV 1/2, have been introduced in rats. rAAV 1/2 (chimeric vector) driven overexpression of A53T α-synuclein in the SN of rats caused a dopaminergic cells loss of 28% at 6 weeks (Koprich et al., 2011). In this study, the choice of the vector titer was crucial, since too high vector titers caused unspecific toxic effects. These second generation rAAV based α-synuclein rat models displayed a more reproducible neurodegeneration (15-60% loss 6-26 weeks p.i.)(Gorbatyuk et al., 2008, Azeredo da Silveira et al., 2009, Sanchez-Guajardo et al., 2010, Koprich et al., 2011). However, even in these rat models, the time course and loss of the nigral TH-positive neurons remained limited and suffered from variability, which hindered observation of clear motor deficits.

Conversely, the consistent and reproducible levels of neurodegeneration achieved in the third generation rAAV model described here were accompanied by robust motor deficits. Dose-dependent impairments of the left forepaw were measured in the cylinder test and could be completely reversed by L-DOPA administration. Using a sensitive rotarod system, a significantly decreased latency time to fall was detected in the rAAV2/7 α-synuclein vector injected animals compared to the rAAV2/7 eGFP control animals. Somewhat surprisingly, the skilled paw reaching test as well as the open field test revealed no significant differences between the rAAV2/7 synuclein and eGFP control animals. The latter results might be explained by the observed low spontaneous exploratory behaviour of the rats compared to mice. Remarkably, the presentation of the motor deficits observed in this rat model was different from those observed in our rAAV-based α-synuclein mouse model (Oliveras-Salva

et al., 2013). rAAV2/7 WT α-synuclein injected mice display a somewhat slower, progressive DA neurodegeneration (up to 80% in the SNpc 8 weeks p.i.) and motor impairments which can be detected from 12 weeks on. The cylinder test performed at 12 weeks p.i. showed only a minor decrease of contralateral forepaw use in mice whereas in our rat model a clear difference of 25% was observed. On the other hand, the open-field test showed significant motor impairments in mice at 16 weeks p.i. unlike in our rat model, where no differences in the open-field test could be observed. Therefore it appears that different behavioural tests might be required to detect motor deficits among different rodent species. The improvements in neurodegeneration and motor deficits observed in this rat model can probably be explained by the choice of the rAAV serotype (rAAV 2/7), the promoter (CMVie-Synapsin1) and the titers and purity of the vector preparation. In line with these results, Decressac et al. reported progressive dopaminergic neurodegeneration up to 75% 8-16 weeks after nigral injection of rAAV2/6 WT α-synuclein using a more efficient rAAV vector construct including the neuron specific synapsin1 promoter (Decressac et al., 2012). We have recently shown that rAAV2/7 vectors outperform most other serotypes in terms of transduction efficiency and expression levels in rat SN (Van der Perren et al., 2011). Using a standard vector dose of rAAV2/7 vectors (3.0E+11 GC/ml), we transduce at least 90% of the nigral DN and probably exceed the crucial threshold of α-synuclein expression necessary to induce profound neuropathology and motor deficits.

Non-invasive imaging of dopaminergic neurodegeneration in pre-clinical rat PD models will facilitate translational research. In this study we used both PET imaging of the dopamine transporter (DAT) binding and MR spectroscopy to study the integrity of the nigrostriatal dopaminergic pathway in our model. In humans, DAT-PET (or SPECT) allows routine assessment of the loss of dopamine transporters in the earliest phase of PD even before the onset of motor symptoms (Brooks et al., 2009, Pavese et al., 2009). We detected the strongest

decrease in DAT binding between 7 and 21 days in the A53T α-synuclein rAAV2/7 injected rats, which is significantly slower than the neurodegeneration induced by 6-OHDA. The use of longitudinal PET imaging in combination with the relatively short-duration of the degeneration process can provide a major advantage for following up of therapeutic interventions in this model. MR spectroscopy was used to non-invasively monitor metabolic changes in the SN. Significantly reduced NAA levels, starting from two weeks after A53T α-synuclein rAAV2/7 injection, confirmed the progressive loss of nigral dopaminergic neurons. Reduction of NAA has also been described in toxin-induced PD models and correlated with the loss of nigral DN (Brownell et al., 1998, Podell et al., 2003, Boska et al., 2005, van Vlieta et al., 2008). In PD patients a wide range of metabolite concentrations is reported, but most studies found decreased NAA concentrations (Clarke et al., 2001, Oz et al., 2006).

Several studies have suggested a role for α-synuclein in the modulation of neurotransmitter release (Bellani et al., 2010). To monitor the effect of α-synuclein overexpression on striatal DA release we performed microdialysis. We observed a time-dependent reduction in both baseline and amphetamine-induced release of DA in the STR after nigral injection of A53T α-synuclein rAAV2/7. Striatal DA release remained TTX-dependent revealing the exocytotic nature of the DA release of the remaining neurons. In comparison with the histological results, we observed earlier defects in striatal DA release (70% reduction) and DA content (60%) compared to the 50% reduction in nigral TH-positive cells and the 50% reduction in DAT binding. These data are in agreement with a recent report by Lundblad and colleagues who used *in vivo* amperometry to examine DA neurotransmission after α-synuclein overexpression with rAAV2/6 (Lundblad et al., 2012). They reported marked changes in DA re-uptake before axonal damage occurred. These data support the hypothesis that Parkinson's disease starts with synaptic dysfunction at the axon terminal level and progresses retrogradely to affect the cell bodies.

Next to dopaminergic neurodegeneration, the presence of α-synucleinopathy is a second important hallmark of PD. Despite the short time course of our model (four weeks), we observed both α-synuclein-positive cytoplasmic aggregates in the SN and dystrophic neurites in the STR. Using a combination of immunohistochemical characterization and western blot analysis of tissue homogenates, we could confirm that α-synuclein becomes phosphorylated, ubiquitinated and insoluble over time. Furthermore, cross-linking of brain homogenates revealed the presence of different α-synuclein species (dimers ≈ 30 kDa and different HMW oligomers ≈ 60kDa and ≈ 85kDa), all indications of a pathological oligomerization and aggregation process.

To date, it remains unclear whether the fibrillar α-synuclein aggregates are neurotoxic *in vivo*. Therefore, we examined the relation between α-synuclein aggregates and nigral neurodegeneration in our model. An initial increase in the percentage of aggregate-positive cells was followed by stabilization at later time points in both the fast and the slow rat model. These data are at odds with the hypothesis that aggregate formation is neuroprotective. Indeed, if α-synuclein aggregates are protective, one would expect to end up with a continuously increasing percentage of aggregate-positive cells. Even when considering the hypothesis that aggregation does not affect cell survival, due to the continuous formation of aggregates, one would expect a continued increase in the percentage of aggregate-positive cells in the final phases instead of a stabilisation as observed in our experiments. The high percentage of aggregate-negative cells we found at later stages implies that aggregate formation processes are deleterious. This conclusion agrees with the observations of Greffard and colleagues, who observed a stable proportion of LB in the SN of PD patients suggesting that LB formation causes neuronal death (Greffard et al., 2010).

In order to reliably translate the results from animal experiments to the human disease, one has to consider the validity of the animal model used. The ideal animal model for PD should

have high face, construct and predictive validity. Face validity needs to be interpreted broadly because behavioral manifestations in rodents and humans always differ. The predictive validity suggests that a treatment that is effective in the model will also be successful in patients. A model based on an established cause of the disease has construct validity and is useful in the understanding of the pathophysiological mechanism. We believe that our α-synuclein rat model shows improved face, construct and predictive validity. The changes that develop in the transduced nigral DN over time, from the early signs of α-synuclein aggregation and impaired DA release, seen at 2 weeks p.i., to the overt cellular pathology and degeneration that develops at 3-4 weeks p.i., support the hypothesis that PD starts with synaptic dysfunction at the axon terminal level and progresses retrogradely to affect the cell bodies. Although the progression in this AAV2/7 α-synuclein model is much faster than in the human disease, the retrograde progression of neurodegeneration mimics the changes described to occur in human PD (Cheng et al., 2010). Furthermore, the consistent and reproducible levels of neurodegeneration achieved in this rat model were accompanied by robust motor deficits which were responsive to L-DOPA treatment. Last, our model is based on overexpression of α-synuclein, a key player in PD pathology. α-Synuclein is the major protein present in LBs in both sporadic and inherited PD and point mutations, duplications and triplications of the *SNCA* gene cause autosomal dominant forms of PD. On the other hand, one has to realize that the α-synuclein inclusions observed in our model do not fully replicate the LB morphology observed in human brain. Also, the involvement of other brain regions in PD brain is not completely recapitulated in our α-synuclein rat model.

We believe that our rAAV2/7 A53T α-synuclein rat model offers new opportunities for preclinical testing of new potential treatments. Furthermore, this rat model will be of great value for further research into the molecular pathogenesis of PD and the importance of α-synuclein aggregation and/or propagation in the disease process.

Acknowledgements

The authors thank Joris Van Asselberghs, Phebe Van Wijk, Peter Vermaelen and Ann Van Santvoort for their excellent technical assistance. Research was funded by the IWT-Vlaanderen (IWT SBO/80020), the FWO Vlaanderen (G.0768.10), by the EC-FP6 program 'DiMI' (LSHB-CT-2005-512146), the FP7 RTD project MEFOPA (HEALTH-2009-241791), the FP7 program 'INMiND' (HEALTH-F2-2011-278850), the KU Leuven (IOF-KP/07/001, OT/08/052A, IMIR PF/10/017), and the MJFox Foundation (Target validation 2010). C. Casteels is a postdoctoral fellow of the Flemish Fund of Scientific Research. K. Van Laere is a senior clinical fellow of the Flemish Fund of Scientific Research. Confocal images were taken in the Cell Imaging Core of the KU Leuven. The authors declare that there is no actual or potential conflict of interest.

References

Anderson, J. P., Walker, D. E., Goldstein, J. M., de Laat, R., Banducci, K., Caccavello, R. J., et al., 2006. Phosphorylation of Ser-129 is the dominant pathological modification of alpha-synuclein in familial and sporadic Lewy body disease. J Biol Chem. 281 (40): 29739-29752.

Appel-Cresswell, S., Vilarino-Guell, C., Encarnacion, M., Sherman, H., Yu, I., Shah, B., et al., 2013. Alpha-synuclein p.H50Q, a novel pathogenic mutation for Parkinson's disease. Mov Disord. 28 (6): 811-813.

Azeredo da Silveira, S., Schneider, B. L., Cifuentes-Diaz, C., Sage, D., Abbas-Terki, T., Iwatsubo, T., et al., 2009. Phosphorylation does not prompt, nor prevent, the formation of alpha-synuclein toxic species in a rat model of Parkinson's disease. Hum Mol Genet. 18 (5): 872-887.

Baekelandt, V., Claeys, A., Eggermont, K., Lauwers, E., De Strooper, B., Nuttin, B., et al., 2002. Characterization of lentiviral vector-mediated gene transfer in adult mouse brain. Hum Gene Ther. 13 (7): 841-853.

Bellani, S., Sousa, V. L., Ronzitti, G., Valtorta, F., Meldolesi, J. and Chieregatti, E., 2010. The regulation of synaptic function by alpha-synuclein. Commun Integr Biol. 3 (2): 106-109.

Boska, M., Lewis, T., Destache, C., Benner, E., Nelson, J., Uberti, M., et al., 2005. Quantitative 1H magnetic resonance spectroscopic imaging determines therapeutic immunization efficacy in an animal model of Parkinson’s disease. Journal of Neuroscience. 25: 1691-1700.

Brooks, D. J. and Pavese, N., 2009. Recent imaging advances in the diagnosis and management of Parkinson's disease. F1000 Med Rep. 1.

Brownell, A., Jenkins, B., Elmaleh, D., Deacon, T., Spealman, R. and Isacson, O., 1998. Combined PET/MRS brain studies show dynamic and long-term physiological changes in a primate model of Parkinson disease. Nature Medicine. 4 (1308-1312).

Casteels, C., Vermaelen, P., Nuyts, J., Van Der Linden, A., Baekelandt, V., Mortelmans, L., et al., 2006. Construction and evaluation of multitracer small-animal PET probabilistic atlases for voxel-based functional mapping of the rat brain. J Nucl Med. 47 (11): 1858-1866.

Chartier-Harlin, M. C., Kachergus, J., Roumier, C., Mouroux, V., Douay, X., Lincoln, S., et al., 2004. Alpha-synuclein locus duplication as a cause of familial Parkinson's disease. Lancet. 364 (9440): 1167-1169.

Cheng, H. C., Ulane, C. M. and Burke, R. E., 2010. Clinical progression in Parkinson disease and the neurobiology of axons. Ann Neurol. 67 (6): 715-725.

Chesselet, M. F., 2008. In vivo alpha-synuclein overexpression in rodents: a useful model of Parkinson's disease? Exp Neurol. 209 (1): 22-27.

Chesselet, M. F. and Richter, F., 2011. Modelling of Parkinson's disease in mice. Lancet Neurol. 10 (12): 1108-1118.

Chung, C. Y., Koprich, J. B., Siddiqi, H. and Isacson, O., 2009. Dynamic changes in presynaptic and axonal transport proteins combined with striatal neuroinflammation precede dopaminergic neuronal loss in a rat model of AAV alpha-synucleinopathy. J Neurosci. 29 (11): 3365-3373.

Clarke, C. and Lowry, M., 2001. Systematic review of proton magnetic resonance spectroscopy of the striatum in parkinsonian syndromes. European Journal of Neurology. 8: 573-577.

Dale, G. E., Probst, A., Luthert, P., Martin, J., Anderton, B. H. and Leigh, P. N., 1992. Relationships between Lewy bodies and pale bodies in Parkinson's disease. Acta Neuropathol. 83 (5): 525-529.

Dawson, T., Mandir, A. and Lee, M., 2002. Animal models of PD: pieces of the same puzzle? Neuron. 35 (2): 219-222.

Dawson, T. M., Ko, H. S. and Dawson, V. L., 2010. Genetic animal models of Parkinson's disease. Neuron. 66 (5): 646-661.

Dawson, V. L., 2000. Neurobiology. Of flies and mice. Science. 288 (5466): 631-632.

Decressac, M., Mattsson, B., Lundblad, M., Weikop, P. and Bjorklund, A., 2012. Progressive neurodegenerative and behavioural changes induced by AAV-mediated overexpression of alpha-synuclein in midbrain dopamine neurons. Neurobiol Dis. 45 (3): 939-953.

Decressac, M., Ulusoy, A., Mattsson, B., Georgievska, B., Romero-Ramos, M., Kirik, D., et al., 2011. GDNF fails to exert neuroprotection in a rat alpha-synuclein model of Parkinson's disease. Brain. 134 (Pt 8): 2302-2311.

Dettmer, U., Newman, A. J., Luth, E. S., Bartels, T. and Selkoe, D., 2013. In vivo cross-linking reveals principally oligomeric forms of alpha-synuclein and beta-synuclein in neurons and non-neural cells. J Biol Chem. 288 (9): 6371-6385.

Eslamboli, A., Romero-Ramos, M., Burger, C., Bjorklund, T., Muzyczka, N., Mandel, R. J., et al., 2007. Long-term consequences of human alpha-synuclein overexpression in the primate ventral midbrain. Brain. 130 (Pt 3): 799-815.

Fleming, S. M., Fernagut, P. O. and Chesselet, M. F., 2005. Genetic mouse models of parkinsonism: strengths and limitations. NeuroRx. 2 (3): 495-503.

Forno, L. S., 1996. Neuropathology of Parkinson's disease. J Neuropathol Exp Neurol. 55 (3): 259-272.

Freichel, C., Neumann, M., Ballard, T., Muller, V., Woolley, M., Ozmen, L., et al., 2007. Age-dependent cognitive decline and amygdala pathology in alpha-synuclein transgenic mice. Neurobiol Aging. 28 (9): 1421-1435.

Gorbatyuk, O. S., Li, S., Sullivan, L. F., Chen, W., Kondrikova, G., Manfredsson, F. P., et al., 2008. The phosphorylation state of Ser-129 in human alpha-synuclein determines

neurodegeneration in a rat model of Parkinson disease. Proc Natl Acad Sci U S A. 105 (2): 763-768.

Greffard, S., Verny, M., Bonnet, A. M., Seilhean, D., Hauw, J. J. and Duyckaerts, C., 2010. A stable proportion of Lewy body bearing neurons in the substantia nigra suggests a model in which the Lewy body causes neuronal death. Neurobiol Aging. 31 (1): 99-103.

Ibanez, P., Bonnet, A. M., Debarges, B., Lohmann, E., Tison, F., Pollak, P., et al., 2004. Causal relation between alpha-synuclein gene duplication and familial Parkinson's disease. Lancet. 364 (9440): 1169-1171.

Izurieta-Sanchez, P., Sarre, S., Ebinger, G. and Michotte, Y., 1998. Effect of trihexyphenidyl, a non-selective antimuscarinic drug, on decarboxylation of L-dopa in hemi-Parkinson rats. Eur J Pharmacol. 353 (1): 33-42.

Kahle, P. J., Neumann, M., Ozmen, L., Muller, V., Odoy, S., Okamoto, N., et al., 2001. Selective insolubility of alpha-synuclein in human Lewy body diseases is recapitulated in a transgenic mouse model. Am J Pathol. 159 (6): 2215-2225.

Kiely, A. P., Asi, Y. T., Kara, E., Limousin, P., Ling, H., Lewis, P., et al., 2013. alpha-Synucleinopathy associated with G51D SNCA mutation: a link between Parkinson's disease and multiple system atrophy? Acta Neuropathol.

Kirik, D., Rosenblad, C., Burger, C., Lundberg, C., Johansen, T. E., Muzyczka, N., et al., 2002. Parkinson-like neurodegeneration induced by targeted overexpression of alpha-synuclein in the nigrostriatal system. J Neurosci. 22 (7): 2780-2791.

Klein, R. L., King, M. A., Hamby, M. E. and Meyer, E. M., 2002. Dopaminergic cell loss induced by human A30P alpha-synuclein gene transfer to the rat substantia nigra. Hum Gene Ther. 13 (5): 605-612.

Koprich, J. B., Johnston, T. H., Huot, P., Reyes, M. G., Espinosa, M. and Brotchie, J. M., 2011. Progressive neurodegeneration or endogenous compensation in an animal model of Parkinson's disease produced by decreasing doses of alpha-synuclein. PLoS One. 6 (3): e17698.

Kruger, R., Kuhn, W., Muller, T., Woitalla, D., Graeber, M., Kosel, S., et al., 1998. Ala30Pro mutation in the gene encoding alpha-synuclein in Parkinson's disease. Nat Genet. 18 (2): 106-108.

Lauwers, E., Beque, D., Van Laere, K., Nuyts, J., Bormans, G., Mortelmans, L., et al., 2007. Non-invasive imaging of neuropathology in a rat model of alpha-synuclein overexpression. Neurobiol Aging. 28 (2): 248-257.

Lauwers, E., Debyser, Z., Van Dorpe, J., De Strooper, B., Nuttin, B. and Baekelandt, V., 2003. Neuropathology and neurodegeneration in rodent brain induced by lentiviral vector-mediated overexpression of alpha-synuclein. Brain Pathol. 13 (3): 364-372.

Lesage, S., Anheim, M., Letournel, F., Bousset, L., Honore, A., Rozas, N., et al., 2013. G51D alpha-synuclein mutation causes a novel parkinsonian-pyramidal syndrome. Ann Neurol.

LeVine, H., 3rd, 1999. Quantification of beta-sheet amyloid fibril structures with thioflavin T. Methods Enzymol. 309: 274-284.

Lo Bianco, C., Deglon, N., Pralong, W. and Aebischer, P., 2004. Lentiviral nigral delivery of GDNF does not prevent neurodegeneration in a genetic rat model of Parkinson's disease. Neurobiol Dis. 17 (2): 283-289.

Lo Bianco, C., Ridet, J. L., Schneider, B. L., Deglon, N. and Aebischer, P., 2002. alpha -Synucleinopathy and selective dopaminergic neuron loss in a rat lentiviral-based model of Parkinson's disease. Proc Natl Acad Sci U S A. 99 (16): 10813-10818.

Löw, K. a. A., P, 2012. Use of viral vectors to create animal models for Parkinson's disease. Neurobiology of disease.

Lundblad, M., Decressac, M., Mattsson, B. and Bjorklund, A., 2012. Impaired neurotransmission caused by overexpression of alpha-synuclein in nigral dopamine neurons. Proc Natl Acad Sci U S A.

Magen, I. and Chesselet, M. F., 2010. Genetic mouse models of Parkinson's disease The state of the art. Prog Brain Res. 184: 53-87.

Maingay, M., Romero-Ramos, M., Carta, M. and Kirik, D., 2006. Ventral tegmental area dopamine neurons are resistant to human mutant alpha-synuclein overexpression. Neurobiol Dis. 23 (3): 522-532.

Marks, W. J., Jr., Bartus, R. T., Siffert, J., Davis, C. S., Lozano, A., Boulis, N., et al., 2010. Gene delivery of AAV2-neurturin for Parkinson's disease: a double-blind, randomised, controlled trial. Lancet Neurol. 9 (12): 1164-1172.

Masliah, E., Rockenstein, E., Mante, M., Crews, L., Spencer, B., Adame, A., et al., 2011. Passive immunization reduces behavioral and neuropathological deficits in an alpha-synuclein transgenic model of Lewy body disease. PLoS One. 6 (4): e19338.

Masliah, E., Rockenstein, E., Veinbergs, I., Mallory, M., Hashimoto, M., Takeda, A., et al., 2000. Dopaminergic loss and inclusion body formation in alpha-synuclein mice: implications for neurodegenerative disorders. Science. 287 (5456): 1265-1269.

Mochizuki, H., Yamada, M. and Mizuno, Y., 2006. Alpha-synuclein overexpression model. J Neural Transm Suppl.(70): 281-284.

Nuber, S., Harmuth, F., Kohl, Z., Adame, A., Trejo, M., Schonig, K., et al., 2013. A progressive dopaminergic phenotype associated with neurotoxic conversion of alpha-synuclein in BAC-transgenic rats. Brain. 136 (Pt 2): 412-432.

Oliveras-Salva, M., Van der Perren, A., Casadei, N., Stroobants, S., Nuber, S., D'Hooge, R., et al., 2013. rAAV2/7 vector-mediated overexpression of alpha-synuclein in mouse substantia nigra induces protein aggregation and progressive dose-dependent neurodegeneration. Mol Neurodegener. 8: 44.

Osorio-Garcia, M., Sima, D., Nielsen, F., Dresselaers, T., Van Leuven, F., Himmelreich, U., et al., 2011. Quantification of in vivo ^{1}H magnetic resonance spectroscopy (MRS) signals with baseline and lineshape estimation. Measurement Science and Technology. 22: 114011.

Osorio-Garcia, M., Sima, D., Nielsen, F., Himmelreich, U. and Van Huffel, S., 2011. Quantification of Magnetic Resonance Spectroscopy signals with lineshape estimation. Journal of Chemometrics. 25: 183-192.

Oz, G., Terpstra, M., Tkac, I., Aia, P., Lowary, J., Tuite, P., et al., 2006. Proton MRS of the unilateral substantia nigra in the human brain at 4 tesla: detection of high GABA concentrations. Magnetic Resonance in Medicine. 55: 296-301.

Pavese, N. and Brooks, D. J., 2009. Imaging neurodegeneration in Parkinson's disease. Biochim Biophys Acta. 1792 (7): 722-729.

Paxinos, G. and Watson, C. 1986. The rat brain in stereotaxic coordinates, Academic Press.

Podell, M., Hadjiconstantinou, M., Smith, M. and Neff, N., 2003. Proton magnetic resonance imaging and spectroscopy identify metabolic changes in the striatum in the MPTP feline model of parkinsonism. Experimental Neurology. 179: 159-166.

Polymeropoulos, M. H., Lavedan, C., Leroy, E., Ide, S. E., Dehejia, A., Dutra, A., et al., 1997. Mutation in the alpha-synuclein gene identified in families with Parkinson's disease. Science. 276 (5321): 2045-2047.

Poullet, J. B., Sima, D. M., Simonetti, A. W., De Neuter, B., Vanhamme, L., Lemmerling, P., et al., 2007. An automated quantitation of short echo time MRS spectra in an open source software environment: AQSES. NMR Biomed. 20 (5): 493-504.

Prasad, K., Tarasewicz, E., Strickland, P. A., O'Neill, M., Mitchell, S. N., Merchant, K., et al., 2011. Biochemical and morphological consequences of human alpha-synuclein expression in a mouse alpha-synuclein null background. Eur J Neurosci. 33 (4): 642-656.

Sanchez-Guajardo, V., Febbraro, F., Kirik, D. and Romero-Ramos, M., 2010. Microglia acquire distinct activation profiles depending on the degree of alpha-synuclein neuropathology in a rAAV based model of Parkinson's disease. PLoS One. 5 (1): e8784.

Sarre, S., Lanza, M., Makovec, F., Artusi, R., Caselli, G. and Michotte, Y., 2008. In vivo neurochemical effects of the NR2B selective NMDA receptor antagonist CR 3394 in 6-hydroxydopamine lesioned rats. Eur J Pharmacol. 584 (2-3): 297-305.

Sarre, S., Vandeneede, D., Ebinger, G. and Michotte, Y., 1998. Biotransformation of L-DOPA to dopamine in the substantia nigra of freely moving rats: effect of dopamine receptor agonists and antagonists. J Neurochem. 70 (4): 1730-1739.

Sarre, S., Yuan, H., Jonkers, N., Van Hemelrijck, A., Ebinger, G. and Michotte, Y., 2004. In vivo characterization of somatodendritic dopamine release in the substantia nigra of 6-hydroxydopamine-lesioned rats. J Neurochem. 90 (1): 29-39.

Schmitz, C. and Hof, P. R., 2005. Design-based stereology in neuroscience. Neuroscience. 130 (4): 813-831.

Shimura, H., Schlossmacher, M. G., Hattori, N., Frosch, M. P., Trockenbacher, A., Schneider, R., et al., 2001. Ubiquitination of a new form of alpha-synuclein by parkin from human brain: implications for Parkinson's disease. Science. 293 (5528): 263-269.

Singleton, A. B., Farrer, M., Johnson, J., Singleton, A., Hague, S., Kachergus, J., et al., 2003. alpha-Synuclein locus triplication causes Parkinson's disease. Science. 302 (5646): 841.

Spillantini, M. G., Schmidt, M. L., Lee, V. M., Trojanowski, J. Q., Jakes, R. and Goedert, M., 1997. Alpha-synuclein in Lewy bodies. Nature. 388 (6645): 839-840.

St Martin, J. L., Klucken, J., Outeiro, T. F., Nguyen, P., Keller-McGandy, C., Cantuti-Castelvetri, I., et al., 2007. Dopaminergic neuron loss and up-regulation of chaperone protein mRNA induced by targeted over-expression of alpha-synuclein in mouse substantia nigra. J Neurochem. 100 (6): 1449-1457.

Taymans, J. M., Vandenberghe, L. H., Haute, C. V., Thiry, I., Deroose, C. M., Mortelmans, L., et al., 2007. Comparative analysis of adeno-associated viral vector serotypes 1, 2, 5, 7, and 8 in mouse brain. Hum Gene Ther. 18 (3): 195-206.

Tofaris, G. K., Garcia Reitbock, P., Humby, T., Lambourne, S. L., O'Connell, M., Ghetti, B., et al., 2006. Pathological changes in dopaminergic nerve cells of the substantia nigra and olfactory bulb in mice transgenic for truncated human alpha-synuclein(1-120): implications for Lewy body disorders. J Neurosci. 26 (15): 3942-3950.

Ulusoy, A., Decressac, M., Kirik, D. and Bjorklund, A., 2010. Viral vector-mediated overexpression of alpha-synuclein as a progressive model of Parkinson's disease. Prog Brain Res. 184: 89-111.

Van der Perren, A., Toelen, J., Carlon, M., Van den Haute, C., Coun, F., Heeman, B., et al., 2011. Efficient and stable transduction of dopaminergic neurons in rat substantia nigra by rAAV 2/1, 2/2, 2/5, 2/6.2, 2/7, 2/8 and 2/9. Gene Ther.

Van der Perren, A., Van den Haute, C. and Baekelandt, V., 2014. Viral Vector-Based Models of Parkinson's Disease. Curr Top Behav Neurosci.

van Vlieta, S., Blezer, E., Jongsma, M., Vanwersch, R., Olivier, B. and Philippens, I., 2008. Exploring the neuroprotective effects of modafinil in a marmoset Parkinson model with immunohistochemistry, magnetic resonance imaging and spectroscopy. Brain Research. 1189: 219-228.

Wilson, A. A., DaSilva, J. N. and Houle, S., 1996. In vivo evaluation of [11C]- and [18F]-labelled cocaine analogues as potential dopamine transporter ligands for positron emission tomography. Nucl Med Biol. 23 (2): 141-146.

Wirdefeldt, K., Adami, H. O., Cole, P., Trichopoulos, D. and Mandel, J., 2011. Epidemiology and etiology of Parkinson's disease: a review of the evidence. Eur J Epidemiol. 26 Suppl 1: S1-58.

Yamada, M., Iwatsubo, T., Mizuno, Y. and Mochizuki, H., 2004. Overexpression of alpha-synuclein in rat substantia nigra results in loss of dopaminergic neurons, phosphorylation of alpha-synuclein and activation of caspase-9: resemblance to pathogenetic changes in Parkinson's disease. J Neurochem. 91 (2): 451-461.

Zarranz, J. J., Alegre, J., Gomez-Esteban, J. C., Lezcano, E., Ros, R., Ampuero, I., et al., 2004. The new mutation, E46K, of alpha-synuclein causes Parkinson and Lewy body dementia. Ann Neurol. 55 (2): 164-173.

Legends

Fig. 1 Stereotactic injection of A53T α-synuclein rAAV2/7 in the SN and STR of the rat induces efficient overexpression of human A53T α-synuclein

(a-b) IHC staining demonstrating α-synuclein overexpression 4 days and 29 days after rAAV mediated transfer in rat SN. Inserts show magnifications of the selected area. Scale bar = 400 µm (overview picture left), 70 µm and 200 µm (inserts right). (c) IHC staining demonstrating eGFP overexpression 4 days and 29 days after rAAV mediated transfer in rat SN. Scale bar = 400 µm. (d, e) Representative confocal images of fluorescent double immunostainings for α-synuclein or eGFP (left) and TH (middle) show extensive co-localization (right) in the transduced region. Scale bar = 50 µm. (f) Stereological quantification of the α-synuclein and eGFP expression volume in the SN at different time points after rAAV2/7 injection (Mean ± s.d., * $p<0.05$ versus 8 days, # $p<0.05$ versus eGFP controls by ANOVA and Bonferroni post hoc test, n= 5). (g) Stereological quantification of the α-synuclein expression volume in the STR at different time points after rAAV2/7 injection (Mean ± s.d., n= 5).

Fig. 2 rAAV 2/7-mediated overexpression of A53T α-synuclein induces dose-dependent dopaminergic cell death and motor deficits

(a, b, c, d) IHC staining for TH in the SN and STR at different time points after injection of (a, b) A53T α-synuclein rAAV2/7 or 29 days after injection of (c, d) eGFP rAAV2/7 in the SN. Scale bar a, c= 400 µm, b, d= 1000 µm. (e) Stereological quantification of the number of TH-positive neurons in the SN over time after A53T α-synuclein rAAV2/7 injection (standard vector dose) or eGFP rAAV2/7 control vector (Mean ± s.d., * $p<0.05$ versus 8 days, # $p<0.05$ versus eGFP controls by ANOVA and Tukey post hoc test, n= 5). (f) Stereological quantification of the number of TH-positive neurons in the SN over time after injection of A53T α-synuclein rAAV2/7 (standard or low vector dose (VD)). (Mean ± s.d., * $p<0.05$

versus 8 days, # $p<0.05$ versus 4 days by ANOVA and Tukey post hoc test, n= 5). (g) Cylinder test at different time points after injection of A53T α-synuclein rAAV2/7 (standard vector dose). (Mean ± s.d., * $p<0.05$ versus 17 days, # $p<0.05$ eGFP controls by ANOVA and Tukey post hoc test, n= 5). (h) Cylinder test at different time points after injection of A53T α-synuclein rAAV2/7 (high vector dose). (Mean ± s.d., * $p<0.05$ by ANOVA and Tukey post hoc test, n= 5). The test was performed with or without administration of L-DOPA (6 mg/kg, i.p.).

Fig. 3 rAAV 2/7-mediated overexpression of A53T α-synuclein induces motor deficits

(a) Open field test at different time points after injection of rAAV 2/7 A53T α-synuclein or rAAV2/7 eGFP (Mean ± s.e.m.). (b) Rotarod test (12-18 rpm) at different time points after injection of rAAV 2/7 A53T α-synuclein or rAAV2/7 eGFP (Mean ± s.e.m.). (c) Rotarod test (4-40 rpm) 6 weeks after injection of rAAV 2/7 A53T α-synuclein or rAAV2/7 eGFP (Mean ± s.e.m., * $p<0.05$). (d) Skilled reach test 6 weeks after injection of rAAV 2/7 A53T α-synuclein or rAAV2/7 eGFP (Mean ± s.e.m.). (e) Cylinder test 6 weeks after injection of rAAV 2/7 A53T α-synuclein or rAAV2/7 eGFP (Mean ± s.e.m., * $p<0.05$)

Fig. 4 Non-invasive imaging of A53T α-synuclein induced dopaminergic cell death using DAT PET

(a-b) Series of horizontal and coronal slices depicting mean striatal DAT binding of (a) A53T α-synuclein rAAV2/7 injected animals (standard vector dose) at different time points after injection (n= 7) and (b) eGFP rAAV 2/7 injected (n= 1) or 6-OHDA treated control animals (n=1) 79 days after injection. Color bars indicate binding potentials for the DAT. (c) Quantification of the DAT impairment of A53T α-synuclein rAAV2/7, eGFP rAAV2/7 and 6-OHDA injected animals followed over time (Mean ± s.d.).

Fig. 5 Non-invasive imaging of A53T α-synuclein induced neurodegeneration using MR spectroscopy.

(a) 3D T2*-weighted MR images (sagittal and coronal view) with an isotropic resolution of 100 μm were used to confirm the location of the rAAV2/7 vector injection. The square box symbolizes the volume of interest (voxel, 2 x 2 x 1.5 mm) for the acquisition of localized 1H MR spectra. MR spectra were acquired for all time points (2, 7, 14, 21 and 35 days p.i.) at the location of the rAAV2/7 vector injection. (b) NAA concentrations of A53T α-synuclein and eGFP injected animals (standard vector dose) were measured over time. The NAA concentrations were quantified by comparison with the unsuppressed water signal. (Data represent mean values ± SD, # $p<0.05$ versus eGFP animals, n=3).

Fig. 6 Nigral overexpression of A53T α-synuclein causes impaired striatal DA release

(a) Mean striatal (STR) DA content in A53T α-synuclein rAAV2/7 injected rats (standard vector dose) as a function of time (Mean ± s.e.m., * $p<0.05$ versus 4 days, # $p<0.05$ versus intact STR by ANOVA followed by Dunnett, n= 4-6). (b) Baseline DA release in A53T α-synuclein rAAV2/7 injected rats as a function of time (Mean ± s.e.m., * $p<0.05$ versus 4 days, by ANOVA followed by Dunnett, n= 4-6). (c) In vivo microdialysis shows effect of amphetamine (AMPH) on extracellular DA release in the STR of α-synuclein rAAV 2/7 injected rats as a function of time. Arrow indicates administration of the drug. The baseline value at time 0 is the mean of 4 values (Mean ± s.e.m., * $p<0.05$ versus baseline value, # $p<0.05$ for 4 day rats versus 15 day rats and 28 day rats after intranigral A53T α-synuclein rAAV2/7 injection by ANOVA for repeated measures followed by Dunnett, n= 4-6). (d) Effect of local perfusion of TTX into the STR on extracellular DA levels in the STR of rats 4 days, 15 days and 28 days following intranigral injection of A53T α-synuclein rAAV2/7

(Mean ± s.e.m.,* $p<0.05$ versus baseline value by ANOVA for repeated measures followed by Dunnett test, n= 4-6).

Fig. 7 Overexpression of A53T α-synuclein induces dose- and time-dependent formation of α-synuclein positive aggregates

(a-b) IHC stainings demonstrate α-synuclein pathology, including (a) cytoplasmic aggregates in the SN and (b) dystrophic and bulging neurites in the STR, after intranigral A53T α-synuclein rAAV2/7 injection (standard vector dose). Top (4 days p.i.) α-synuclein positive cells and neurites without aggregates and bottom (17 days p.i.) with aggregates (arrows). Scale bar A, B= 10 µm. (c) Representative confocal images of fluorescent double immunostainings for α-synuclein (green) and ubiquitin (red) show an increase in co-localization over time (arrows). Scale bar c= 50 µm. (d) Thioflavin S staining of SN 4 and 29 days after injection of A53T α-synuclein rAAV2/7. Scale bar D=30 µm. (e) IHC staining against P-S129 α-synuclein at different time points. (f) Representative confocal image of fluorescent double immunostaining for P-S129 α-synuclein (green) and TH (red) show co-localization in DN. Scale bar = 20 µm. (g) Stereological quantification of the number of P-S129 α-synuclein positive cells in the SN of rats injected with A53T α-synuclein rAAV2/7 (Mean ± s.d., * $p < 0.05$ by ANOVA and Tukey post hoc test, n= 5). (h, k) Stereological quantification of the number of α-synuclein positive cells in the SN of rats injected with a standard (h) or low (k) vector dose of A53T α-synuclein rAAV2/7 (Mean ± s.d., * $p < 0.05$ by ANOVA and Tukey post hoc test, n= 5). (i, l) The percentage of aggregate-positive cells in the SN of rats injected with a standard (i) or low (l) vector dose of A53T α-synuclein rAAV2/7. (Mean ± s.d., * $p < 0.05$ by ANOVA and Tukey post hoc test, n= 5). (j, m) Absolute number of α-synuclein positive cells in the SN with and without aggregates of rats

injected with a standard (j) or low (m) vector dose of A53T α-synuclein rAAV2/7 (Mean ± s.d., * $p < 0.05$ by ANOVA and Tukey post hoc test, n= 5).

Fig. 8 Overexpression of A53T α-synuclein induces insoluble α-synuclein positive aggregates.

(a, b, c) Immunoblot analysis of soluble fraction of nigral tissue extracts of A53T α-synuclein rAAV2/7 injected rats (standard vector dose). For detection of α-synuclein a rodent-specific antibody or an antibody against phosphorylated α-synuclein was used. An antibody against β-actin was used as internal loading control. (d, e) Immunoblot analysis of insoluble fraction of nigral tissue extracts of A53T α-synuclein rAAV2/7 injected animals. For detection of α-synuclein a human-specific antibody was used. Quantitative analysis was based on densitometry, the protein levels of 3 independent blots and presented relative to β-actin levels (Mean ± s.e.m., *$p < 0.05$, ** $p < 0.01$, *** $p < 0.001$ by ANOVA and Tukey post hoc test). (f) Immunoblot analysis of nigral tissue extracts of A53T α-synuclein rAAV2/7 (standard vector dose) animals 7 days and 28 days p.i. as well as non-injected animals (NI) using crosslinking. For detection of α-synuclein a human-specific antibody (15G7) was used.

Supplemental Fig. 1 Determination of endogenous and overexpressed levels of α-synuclein in vivo.

Immunoblot analysis of nigral tissue extracts of A53T α-synuclein rAAV2/7 injected rats (standard vector dose) 7 days and 28 days p.i.. For detection of both rat and human α-synuclein an in house antibody against α-synuclein was used. An antibody against α-tubulin was used as internal loading control. NI = non-injected animals, n= 2-3.

Supplemental Fig. 2 rAAV 2/7-mediated overexpression of A53T α-synuclein induces dopaminergic cell death

IHC staining for TH, VMAT2 and Nissl staining in the SN after injection of rAAV2/7 A53T α-synuclein 29 days post injection. NI = non-injected side, I = injected side. Upper panel overview picture of the SN, lower panel detailed zoom in. Scale bar upper panel = 500 µm, Scale bar lower panel= 100 µm.

Supplemental Fig. 3 rAAV 2/7-mediated overexpression of WT α-synuclein induces dopaminergic cell death and motor deficits.

(a) Stereological quantification of the number of TH-positive neurons in the SN over time after WT α-synuclein rAAV2/7 injection (8.0E+11 GC/ml) (Mean ± SD, * $p<0.05$, n= 4). (b) Cylinder test at different time points after injection of WT α-synuclein rAAV2/7. (Mean ± SD, * $p<0.05$, n= 4).

Supplemental Fig. 4 MR imaging and MR spectroscopy in A53T α-synuclein rAAV2/7 injected animals.

(a) T2-weighted spin echo and (b) T2*-weighted gradient echo. MRI in rAAV2/7 injected animals showing the injection site with (a) edema (b) and hemorrhage/ bleedings close to the skull (arrow). (c-d) MR spectroscopy quantifies glutamate and GABA concentrations in comparison with the unsuppressed water signal. (Mean ± SD)

Supplemental Fig. 5 α-synuclein overexpression preferentially kills dopaminergic neurons.

Representative confocal image of fluorescent double immunostaining for TH and NeuN in the SN of rAAV2/7 α-synuclein injected animals 28 days p.i. . Scale bar = 20 µm.

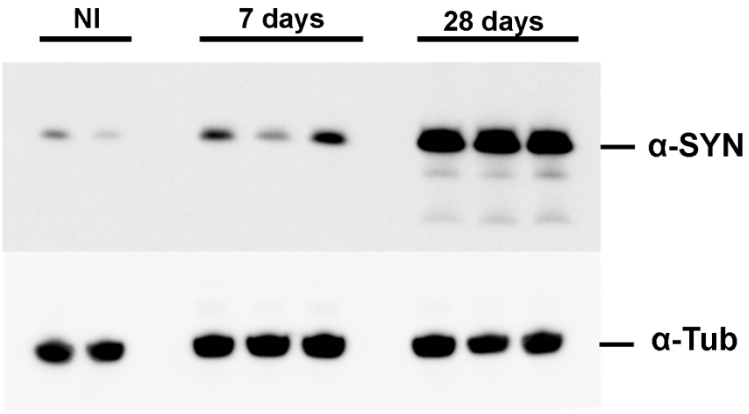

Supplemental Fig. 1 Determination of endogenous and overexpressed levels of α-synuclein in vivo.

Immunoblot analysis of nigral tissue extracts of A53T α-synuclein rAAV2/7 injected rats (standard vector dose) 7 days and 28 days p.i.. For detection of both rat and human α-synuclein an in house antibody against α-synuclein was used. An antibody against α-tubulin was used as internal loading control. NI = non-injected animals, n= 2-3.

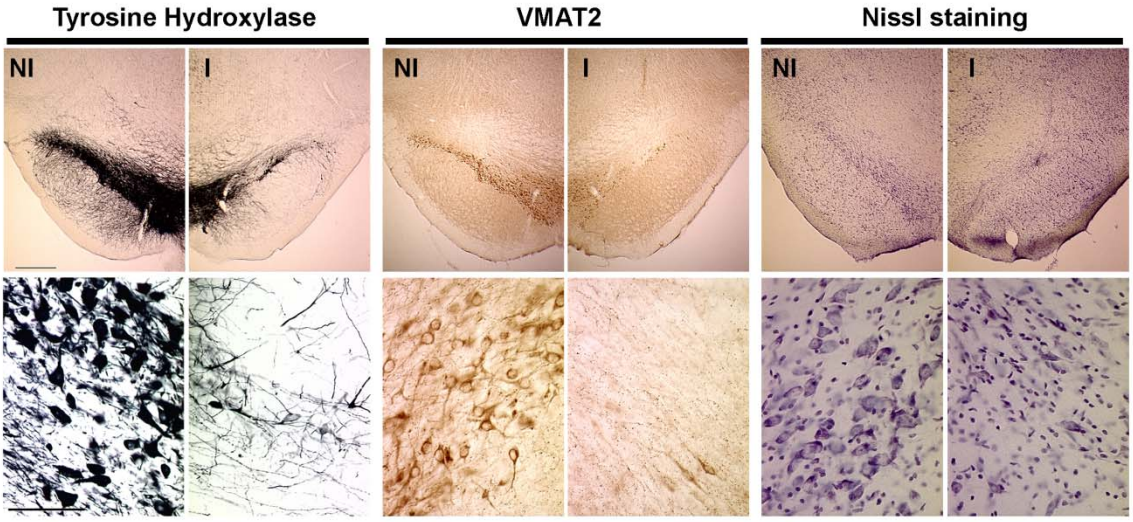

Supplemental Fig. 2 rAAV 2/7-mediated overexpression of A53T α-synuclein induces dopaminergic cell death

IHC staining for TH, VMAT2 and Nissl staining in the SN after injection of rAAV2/7 A53T α-synuclein 29 days post injection. NI = non-injected side, I = injected side. Upper panel overview picture of the SN, lower panel detailed zoom in. Scale bar upper panel = 500 µm, Scale bar lower panel= 100 µm.

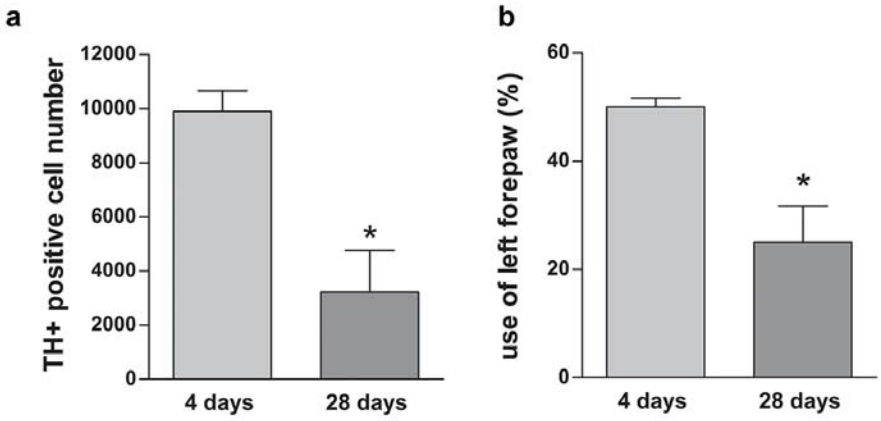

Supplemental Fig. 3 rAAV 2/7-mediated overexpression of WT α-synuclein induces dopaminergic cell death and motor deficits.

(a) Stereological quantification of the number of TH-positive neurons in the SN over time after WT α-synuclein rAAV2/7 injection (8.0E+11 GC/ml) (Mean ± SD, * $p<0.05$, n= 4). (b) Cylinder test at different time points after injection of WT α-synuclein rAAV2/7. (Mean ± SD, * $p<0.05$, n= 4).

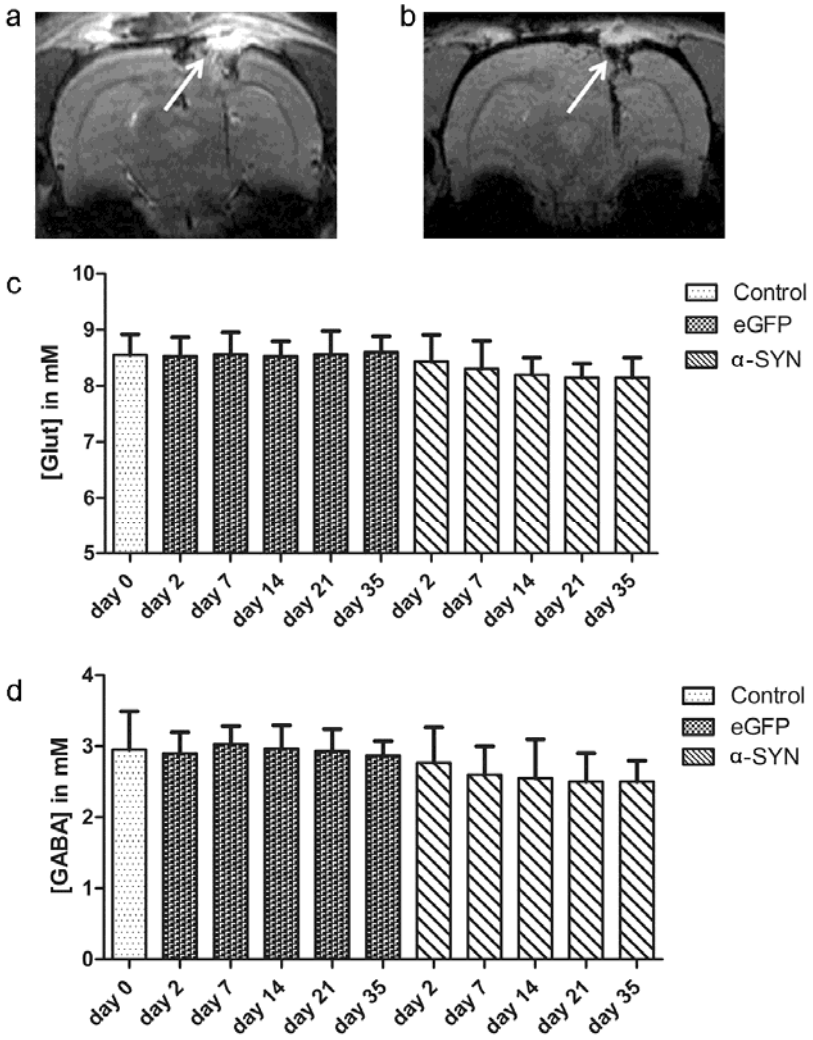

Supplemental Fig. 4 MR imaging and MR spectroscopy in A53T α-synuclein rAAV2/7 injected animals.

(a) T2-weighted spin echo and (b) T2*-weighted gradient echo. MRI in rAAV2/7 injected animals showing the injection site with (a) edema (b) and hemorrhage/ bleedings close to the skull (arrow). (c-d) MR spectroscopy quantifies glutamate and GABA concentrations in comparison with the unsuppressed water signal. (Mean ± SD)

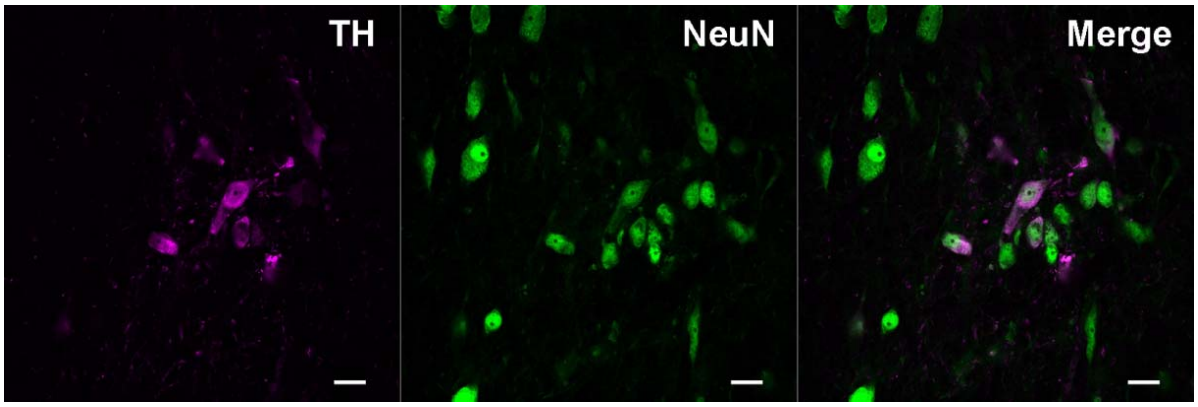

Supplemental Fig. 5 α-synuclein overexpression preferentially kills dopaminergic neurons.

Representative confocal image of fluorescent double immunostaining for TH and NeuN in the SN of rAAV2/7 α-synuclein injected animals 28 days p.i. . Scale bar = 20 µm.

Figures

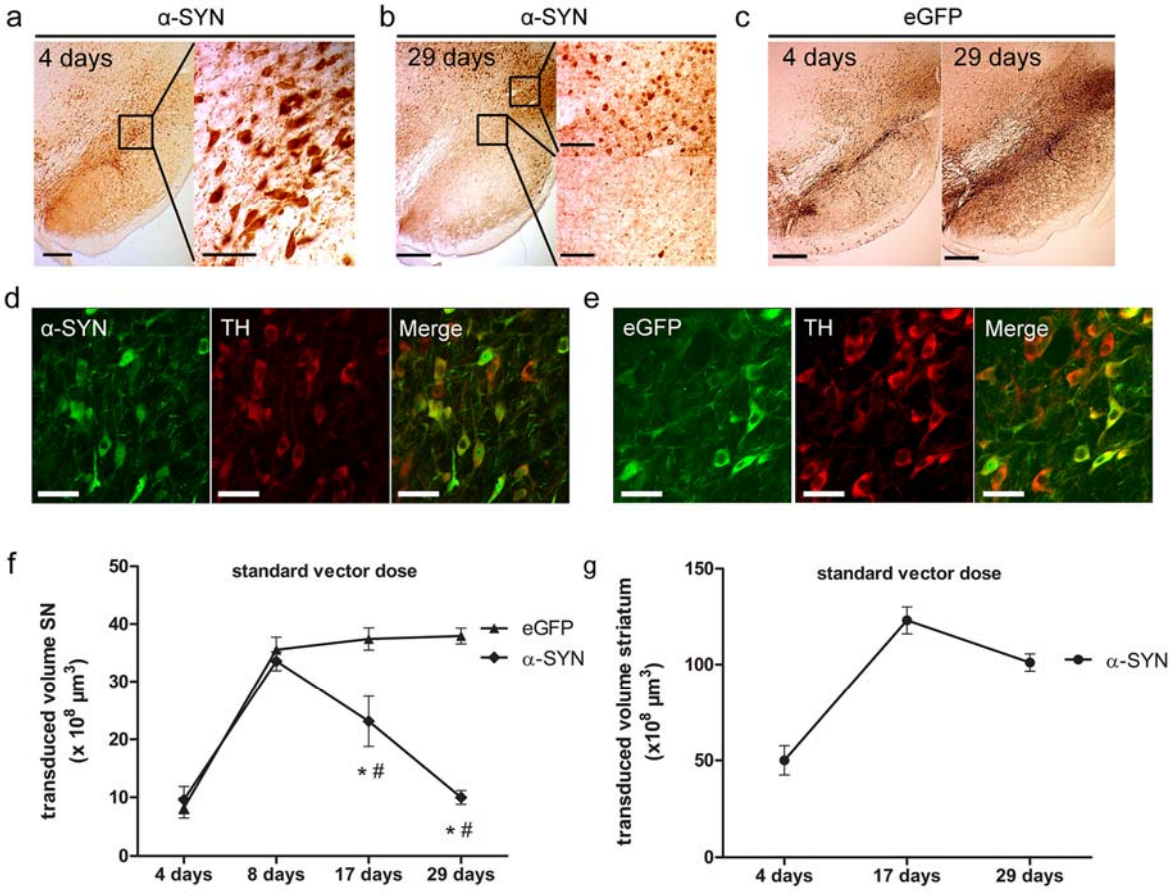

Fig. 1 Stereotactic injection of A53T α-synuclein rAAV2/7 in the SN and striatum of the rat induces efficient overexpression of human A53T α-synuclein

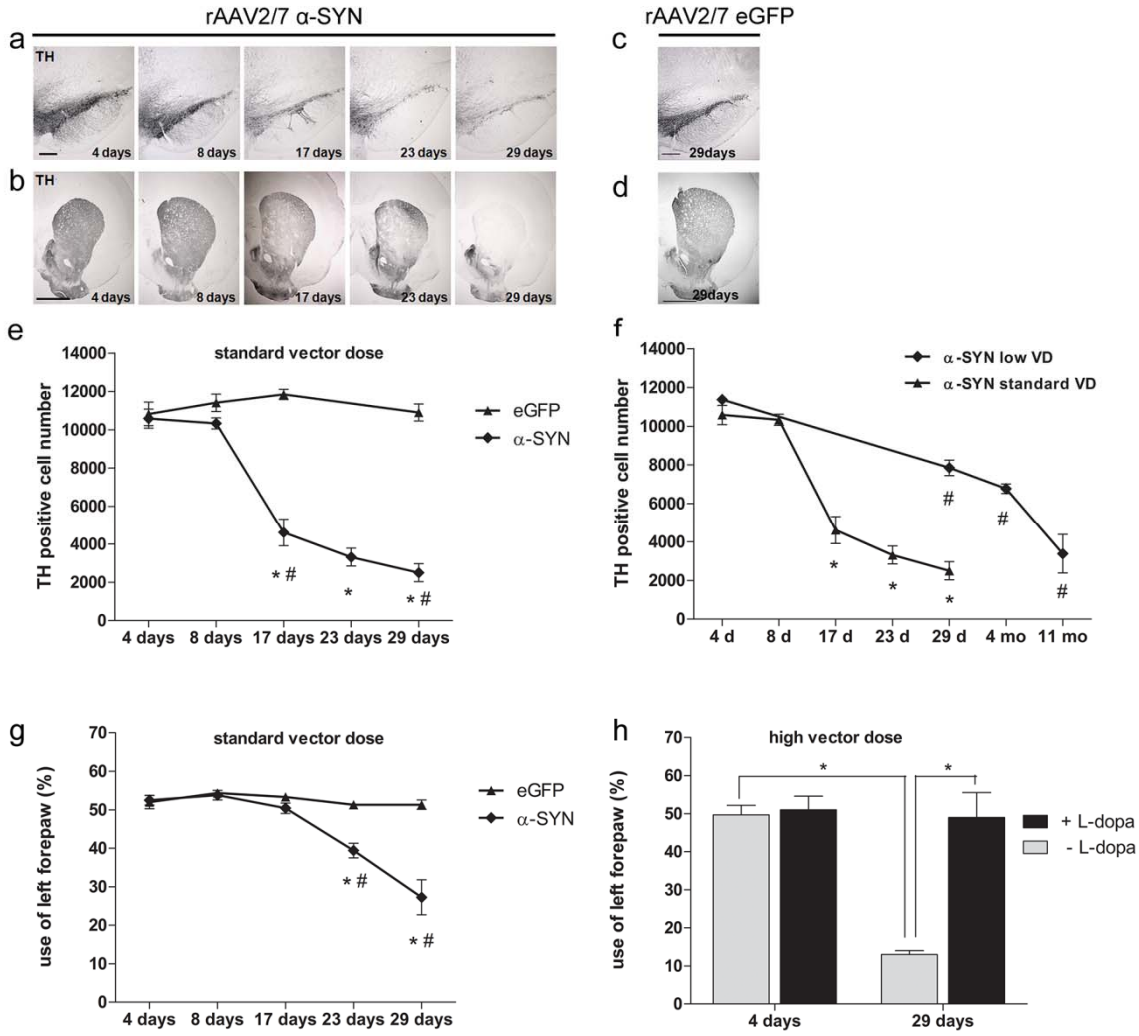

Fig. 2 rAAV 2/7-mediated overexpression of A53T α-synuclein induces dose-dependent dopaminergic cell death and motor deficits

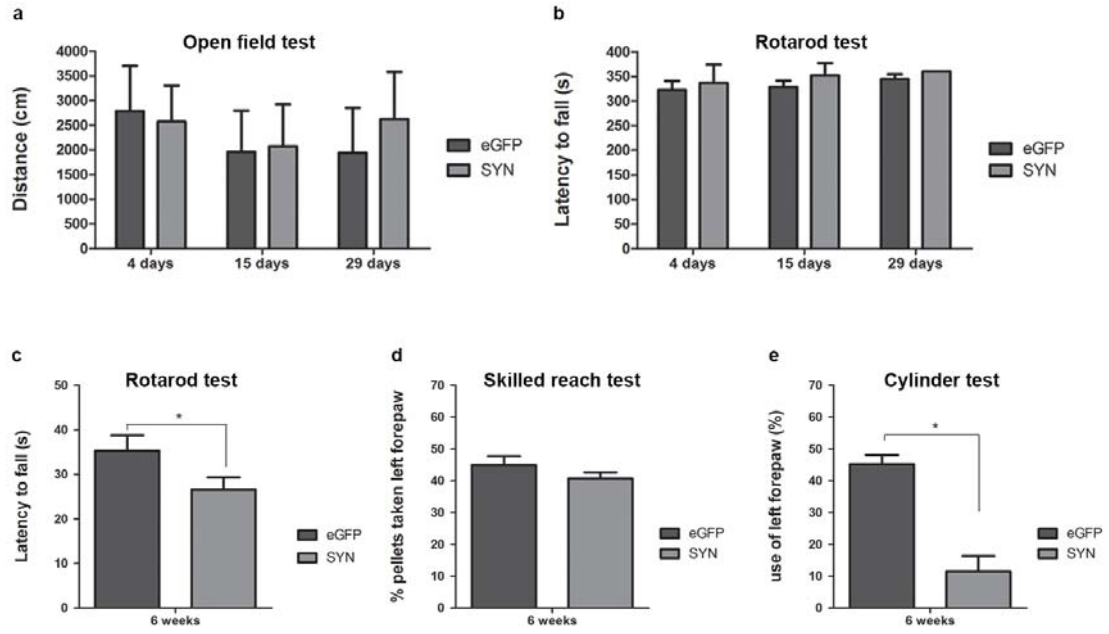

Fig. 3 rAAV 2/7-mediated overexpression of A53T α-synuclein induces motor deficits

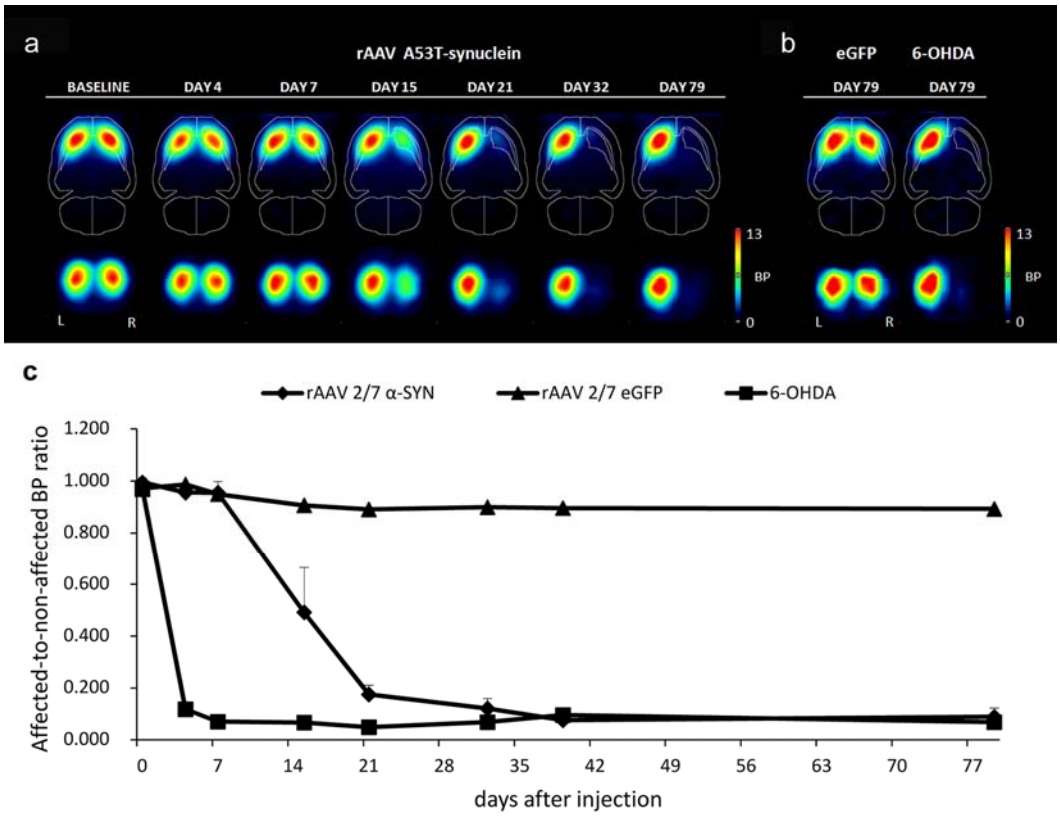

Fig. 4 Non-invasive imaging of A53T α-synuclein induced dopaminergic cell death using DAT PET

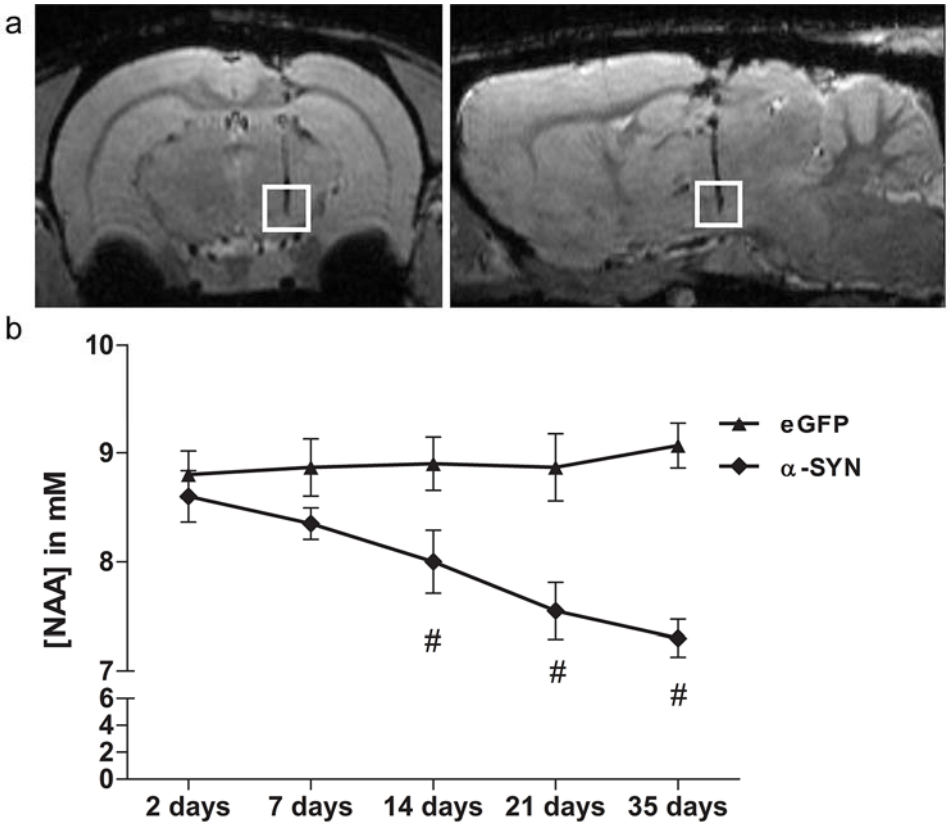

Fig. 5 Non-invasive imaging of A53T α-synuclein induced neurodegeneration using MR spectroscopy.

a

	DA content denervated STR (ng/g)	DA content intact STR (ng/g)
4 days	6284 ± 943	6669 ± 1197
15 days	2413 ± 449 * #	6190 ± 816
28 days	524 ± 92 * #	6969 ± 751

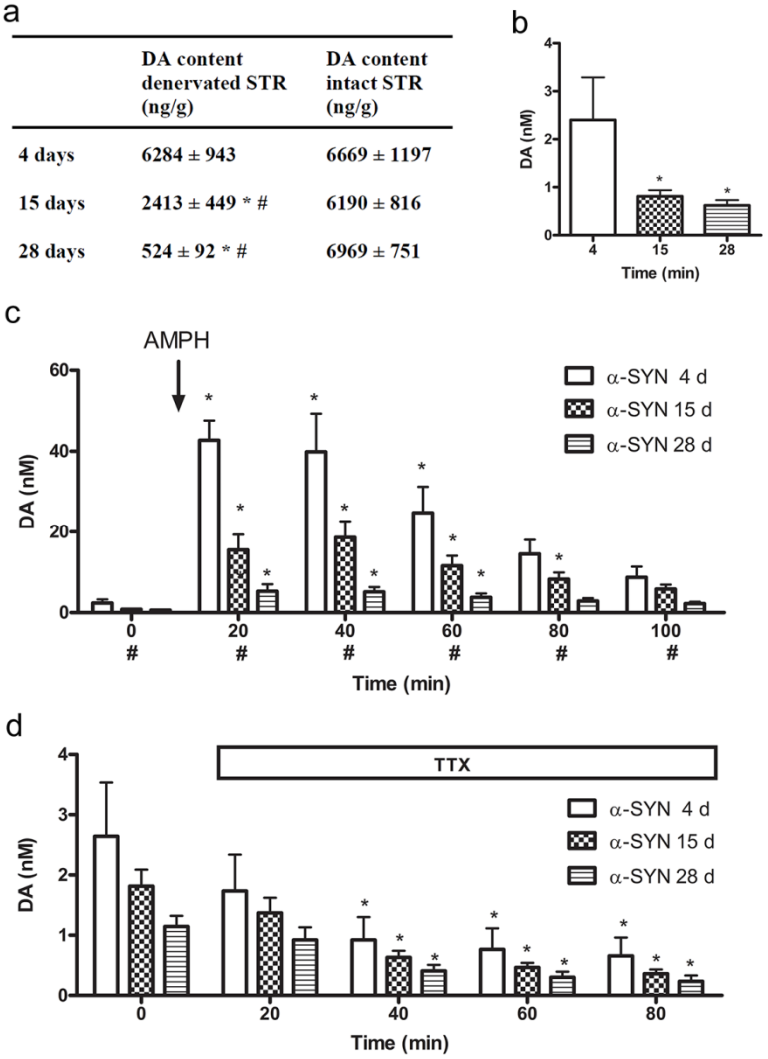

Fig. 6 Nigral overexpression of A53T α-synuclein causes impaired striatal DA release

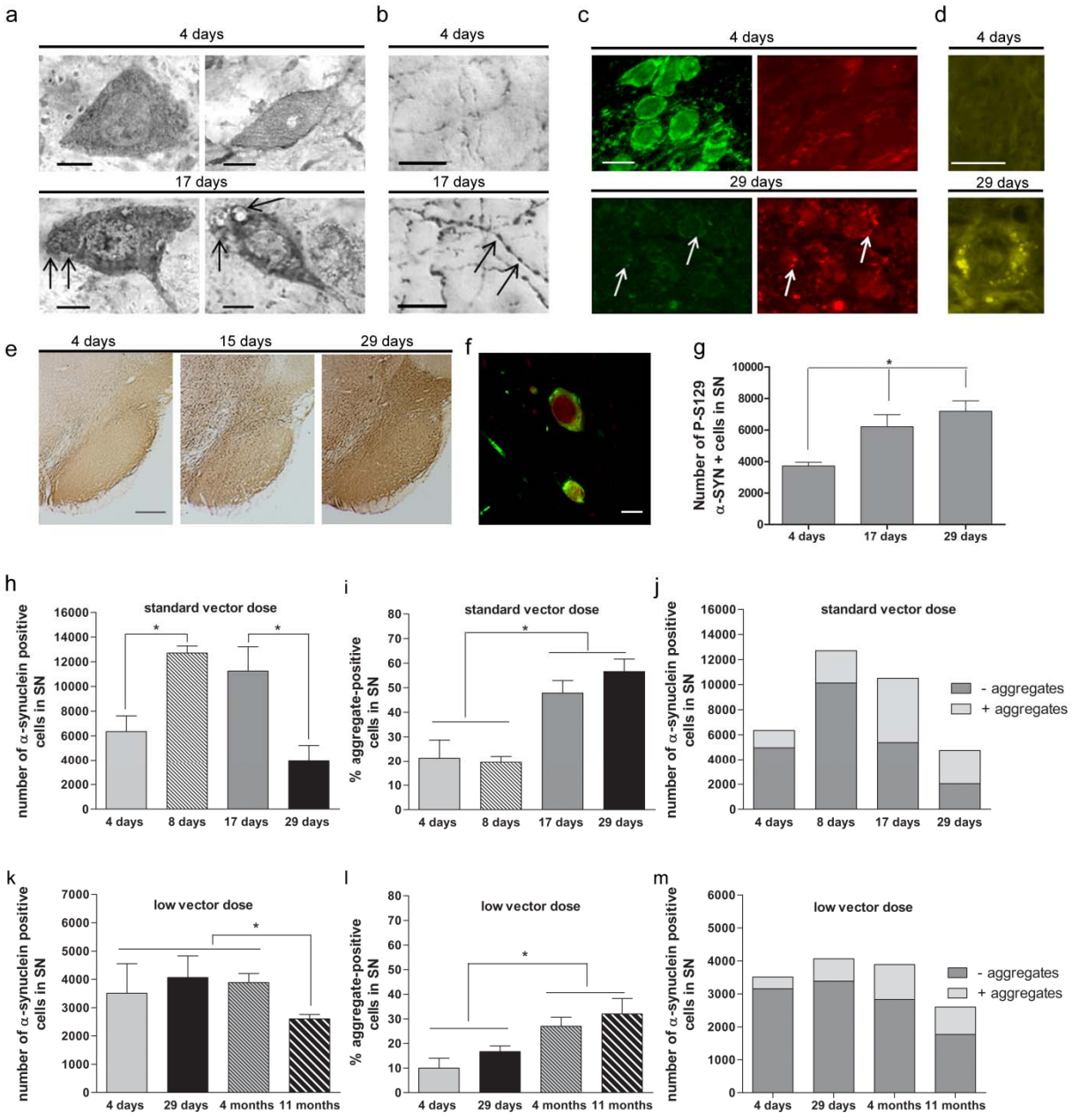

Fig. 7 Overexpression of A53T α-synuclein induces dose- and time-dependent formation of α-synuclein positive aggregates

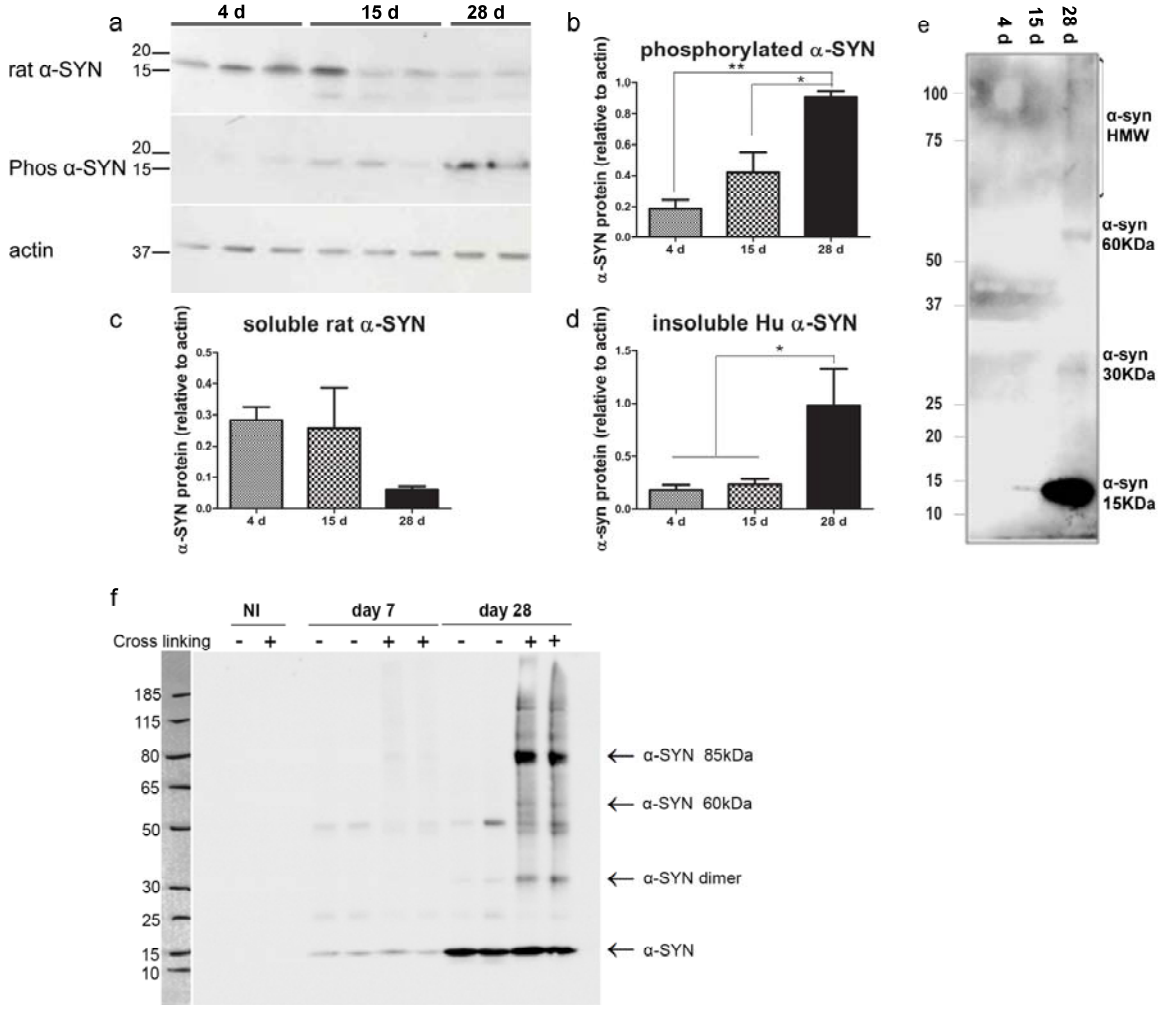

Fig. 8 Overexpression of A53T α-synuclein induces insoluble α-synuclein positive aggregates.